Capture and imaging of a prehairpin fusion intermediate of the paramyxovirus PIV5

Yong Ho Kim[a], Jason E. Donald[b], Gevorg Grigoryan[b,1], George P. Leser[c], Alexander Y. Fadeev[d], Robert A. Lamb[c,2], and William F. DeGrado[a,b,2,3]

[a]Department of Chemistry, University of Pennsylvania, Philadelphia, PA 19104; [b]Department of Biochemistry and Biophysics, University of Pennsylvania, Philadelphia, PA 19104; [c]Howard Hughes Medical Institute and Department of Molecular Biosciences, Northwestern University, Evanston, IL 60201; and [d]Department of Chemistry and Biochemistry, Seton Hall University, South Orange, NJ 07079

Contributed by William F. DeGrado, October 11, 2011 (sent for review August 26, 2011)

During cell entry, enveloped viruses fuse their viral membrane with a cellular membrane in a process driven by energetically favorable, large-scale conformational rearrangements of their fusion proteins. Structures of the pre- and postfusion states of the fusion proteins including paramyxovirus PIV5 F and influenza virus hemagglutinin suggest that this occurs via two intermediates. Following formation of an initial complex, the proteins structurally elongate, driving a hydrophobic N-terminal "fusion peptide" away from the protein surface into the target membrane. Paradoxically, this first conformation change moves the viral and cellular bilayers further apart. Next, the fusion proteins form a hairpin that drives the two membranes into close opposition. While the pre- and postfusion hairpin forms have been characterized crystallographically, the transiently extended prehairpin intermediate has not been visualized. To provide evidence for this extended intermediate we measured the interbilayer spacing of a paramyxovirus trapped in the process of fusing with solid-supported bilayers. A gold-labeled peptide that binds the prehairpin intermediate was used to stabilize and specifically image F-proteins in the prehairpin intermediate. The interbilayer spacing is precisely that predicted from a computational model of the prehairpin, providing strong evidence for its structure and functional role. Moreover, the F-proteins in the prehairpin conformation preferentially localize to a patch between the target and viral membranes, consistent with the fact that the formation of the prehairpin is triggered by local contacts between F- and neighboring viral receptor-binding proteins (HN) only when HN binds lipids in its target membrane.

fusion protein refolding | membrane fusion | electron microscopy

Enveloped viruses such as influenza virus, human immunodeficiency virus (HIV), and parainfluenza virus 5 (PIV5) encode class I fusion proteins that mediate coalescence of the viral and target membranes (1–6). Homotrimeric class I fusion proteins are synthesized as biologically inactive precursors that are activated by proteolytic cleavage, which generates a new N-terminal hydrophobic sequence known as the fusion peptide. The crystal structures of the paramyxovirus F-protein in its metastable prefusion form and the human parainfluenza virus 3 (hPIV3) F-protein in its very stable postfusion form, and also the influenza virus HA in pre- and postfusion conformations, reveal a unique protein architecture that undergoes large-scale, irreversible refolding during membrane fusion (7–10).

These structures provided snapshots of the locations of the critical fusion peptide in the initial and final states: In the prefusion form, the fusion peptide is located along the protein surface, near the virus membrane; while in the postfusion state it is positioned to penetrate into the viral membrane through the formation of a hairpin conformation. Nevertheless, photochemical labeling (11) indicates that the fusion peptide engages with the target membrane in an intermediate state known as the "prehairpin" state. This prehairpin state has been hypothesized to be a highly extended parallel coiled coil, which drives the fusion peptide beyond the surface of the virus to allow it to insert deeply into the target membrane. Interestingly, this conformational change would be expected to drive the membranes further apart than in the initial complex, due to the proposed elongated nature of the prehairpin. Next, the formation of the final hairpin form is hypothesized to drive the close apposition of the bilayers required for fusion to proceed. The hypothetical extended prehairpin form has served as a remarkably robust model for the design of peptide drugs that inhibit HIV and PIV5 fusion such as T-20 and C1 (12–14). However, to date, the existence of this prehairpin intermediate has been shown only indirectly (15–17). Direct observation of this state would be a valuable test of current models of viral fusion and the mode of action of entry inhibitors.

Here we characterize the prehairpin intermediate of a paramyxovirus, which fuses with the cytoplasmic membrane and does not require endocytosis or low pH-triggering (2). The initial binding occurs via transient interactions between its receptor-binding protein known as hemagglutinin-neuraminidase (HN) and sialic acid moieties on the cell surface. The engagement of HN with its substrate leads to conformational changes in neighboring F-proteins on the viral envelope, which then convert to the prehairpin form. We built a computational model for F in this metastable intermediate, which predicted a relatively long bilayer-to-bilayer spacing of 21 nm. We used electron microscopy (EM) to characterize the fusion of virions with nano-bead supported bilayers (18), which were expected to be less deformable than liposomes or cells and hence slower to fuse with virus. A previously characterized prehairpin-binding peptide was used to further trap this intermediate and enable immuno-gold labeling. Direct measurement of the interbilayer distance shows that the separation closely matches that predicted from the computational model for the prehairpin intermediate. Additionally, the F-proteins in the prehairpin state on the surface of the virus specifically localize to the contact area between the virus and the target membrane. These experiments provide direct evidence for this prehairpin intermediate in an intact cell, and suggest that the fusion protein does travel through this large, extended intermediate state on the path to fusion.

Results and Discussion

A Computational Modeling of the Prehairpin Intermediate State. An atomic-scale model was constructed to determine the overall

Author contributions: Y.H.K., J.E.D., A.Y.F., R.A.L., and W.F.D. designed research; Y.H.K., J.E.D., and G.G. performed research; Y.H.K., J.E.D., G.G., and A.Y.F. contributed new reagents/analytic tools; Y.H.K., J.E.D., G.G., G.P.L., R.A.L., and W.F.D. analyzed data; and Y.H.K., J.E.D., R.A.L., and W.F.D. wrote the paper.

The authors declare no conflict of interest.

[1]Present address: Department of Computer Science, Dartmouth College, Hanover, NH 03755.

[2]To whom correspondence may be addressed. E-mail: ralamb@northwestern.edu or william.degrado@ucsf.edu.

[3]Present address: Department of Pharmaceutical Chemistry, University of California, San Francisco, San Francisco, CA 94143.

This article contains supporting information online at www.pnas.org/lookup/suppl/doi:10.1073/pnas.1116034108/-/DCSupplemental.

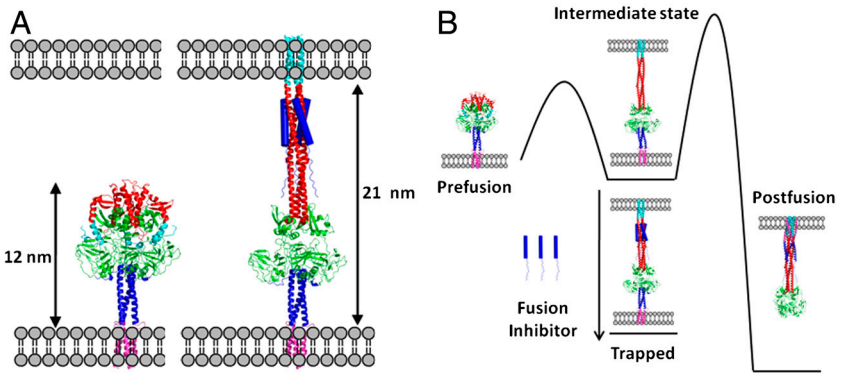

Fig. 1. Structures of the fusion protein in fusion states and their thermodynamics. (*A*) Models of the prefusion (7, 27) (left) and the prehairpin intermediate bound by the fusion inhibitor (right) show the distance expected to be observed in EM. The fusion peptide is shown in cyan, heptad repeat A in red, the globular head domain in green, heptad repeat B in dark blue (cartoon), and the TM domain in magenta. The fusion-inhibitory peptide, C1 (12), is shown in dark blue (filled cylinders). (*B*) Schematic diagram illustrating the free energy changes in the system. The canonical pathway moves from prefusion, to the intermediate state, through a high barrier to the postfusion state (8). Introduction of the fusion-inhibitory peptide, C1, traps the protein in the intermediate state conformation (12).

length of the aqueous domain, and hence the expected interbilayer distance of the intermediate. Type I fusion proteins, including PIV5 F, influenza virus HA, and HIV Env, have two helical repeat (HRA and HRB) regions that form coiled coils during different stages of fusion. In the prefusion state of PIV5, HRA lies along the protein surface, while HRB forms a trimeric coiled coil stalk adjacent to the viral membrane (7). In the prefusion state, HRA is believed to detach from the protein surface and refold into a long, extended three-stranded coiled coil projecting towards the target bilayer, while HRB remains essentially intact and anchored near the virus surface. During formation of the hairpin intermediate, the HRA trimer remains constant, while the original HRB bundle dissociates and its individual chains bind along the exterior of the HRA trimer, pulling the viral membrane toward the target bilayer until the postfusion trimer of helical hairpins is fully formed (8, 19). Thus, the prehairpin intermediate shows hybrid character, having HRA and HRB in the starting and postfusion conformations, respectively. One domain of F (residues 290–357) is largely invariant in the pre- and postfusion structures; it appears to form a hinged hub about which HRA and HRB pivot during these conformational rearrangements. Thus, by superposing this domain in the pre- and postfusion states, it was possible to define the positions of HRA and HRB in the prehairpin intermediate (see *Methods* and *Dataset S1*). The end-to-end distance of the resulting model (Fig. 1 *A* and *B*) is 21 nm with an associated error of approximately 1 nm, primarily reflecting the error in predicting where the transmembrane (TM) and fusion peptides enter the membranes.

Bilayer-Supported Silica and Polystyrene Nanobeads. For microscopic studies, lipid bilayers were supported on nanosilica or polystyrene (PS) nanobeads. The silica-supported bilayers maintain, by tethering the bilayer to the nanobead with poly(ethylene glycol) (PEG), an internal space that allows for incorporation of membrane proteins containing cytoplasmic domains. For experiments requiring thin-sectioning we used the softer polystyrene (PS) as the support. An electron micrograph (Fig. S1) shows the structure of silica and PS nanobeads stained using a mixture of 2% uranyl acetate and 2% osmium tetroxide. The membrane surface of the silica-supported nanobeads is approximately 50 Å from the nanobead core because of the flexible PEG linkages, as compared to the 40 Å that would be observed if the membrane was directly on the surface of the solid support. To control the size homogeneity, curvature of membranes, and structural properties of the nanobeads, 100–150 nm silica and ≈120 nm polystyrene beads (average diameter) were selected.

To induce fusion of PIV5 particles (virons) with nanobead-supported bilayers, the bilayer was modified with sialoganglioside to serve as a receptor for binding by the PIV5 attachment protein, HN. PIV5 HN binding to sialic acid is believed to lead to activation of F-protein, priming the conformational transition from the prefusion state to intermediates along the fusion reaction pathway (20, 21).

Fusion Between Viruses and Nanobead-Supported Bilayers. For paramyxoviruses, binding of virus to surface sialic acids at 37 °C to 42 °C triggers the conformational changes leading to fusion (22, 23). As expected, fusion was observed at 37° and 42 °C by EM

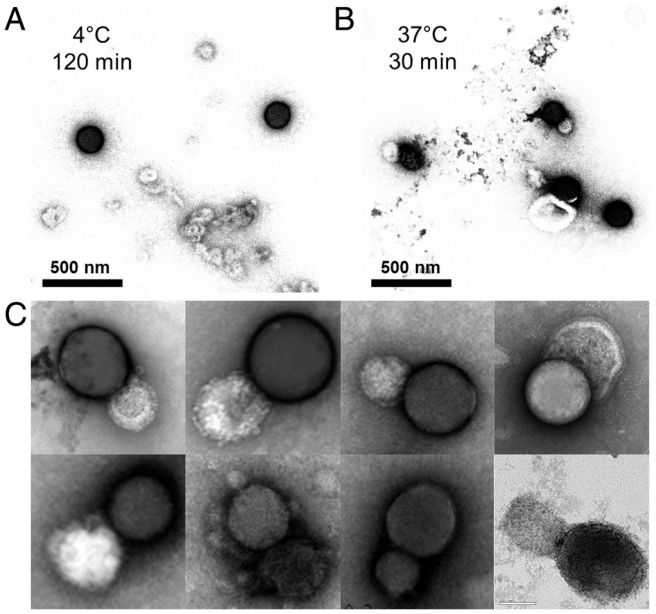

Fig. 2. Temperature triggers viral fusion with nanobead-supported bilayers. EM images of the samples. (*A*) At 4 °C, nanobead-supported bilayers made up of silica nanobeads were combined with purified PIV5 particles that express the fusion (F) protein spike on their surface. At this temperature there is little association between the virus and the nanobead-supported bilayers. Dark spheres represent silica nanobead and light vesicles are viruses. Silica-supported bilayers appear darker under these conditions. (*B*) After warming to 37 °C for 30 min viral particles fuse to nanobead-supported bilayers. Samples in (*A* and *B*) were stained with 4% uranyl acetate. (*C*) EM gallery of fused virus/nanobead-supported bilayers pairs in higher magnification. PIV5 virions with a concentration of 1.0×10^{10} plaque forming units (PFU)/mL were mixed with silica nanobeads with an approximate concentration of 5×10^9 particles/mL into 100 μL total volumes and incubated at the desired temperature. The concentration of silica nanobeads was calculated from weight, assuming a 120 nm mean diameter of silica and its density of 2.2 g/cm^3.

after 30 min incubation (Fig. 2*B*), but not at 4 °C and 25 °C (Fig. 2*A*). Darker, nanobead-supported bilayers are readily distinguished from the virus particles.

Measurement of the Spacing Between Viral Membranes and Nanobead-Supported Bilayers. The computational model predicts a bilayer separation of 21 nm in the prehairpin intermediate (Fig. 1*A*). Using thin-sectioning EM with staining allowed the surface spike glycoproteins of PIV5 to be observed. To trap the F-protein in the prehairpin conformation, we included an inhibitory peptide, C-1, derived from the HRB region of F (12). The C-1 peptide binds specifically to the prehairpin form of F, and is believed to inhibit PIV5 fusion by trapping the protein in this state and preventing it from proceeding to the final hairpin form (Fig. 3*A*). More than 150 images of virus/nano-particle mimic pairs were analyzed. In both the presence and absence of the fusion inhibitor, the distance between the viral and nanobead-supported bilayer was measured (Fig. 3 *A* and *D*). Unlike unsectioned silica nanobead-supported samples (Fig. 2), the contrast of sectioned samples (Fig. 3) resulted in the viruses being more darkly stained due to the internal ribonucleoprotein core. In the absence of the fusion-inhibitory peptide, fusion was observed (Fig. 3*D*) and most virus/nanobead-supported bilayer pairs are separated by a short distance (Fig. 3*C*). In the presence of the fusion-inhibitory peptide, the distribution of interparticle distances peaked at approximately 20 nm (Fig. 3*C*), very closely matching the value predicted by the computational model (Fig. 1*A*).

The conformation of the trapped prehairpin intermediate is suggested by significant changes of proteins adjacent to the nanobead-supported bilayer surface (Fig. 3 *A* and *B*). While regions of the virus far from the interface show densely packed protein (presumably a mixture of HN and F in its prefusion conformation, blue arrows, Fig. 3*B*), regions close to the interface appear to be less densely packed, (yellow arrows, Fig. 3*B*) consistent with a transition between the prefusion conformation and the prehairpin intermediate (Fig. 3*B*).

Immuno-Gold Labeling Shows Localization of Inhibited PIV5 F-Protein to the Interfacial Region. We next localized the proteins that had reached the prehairpin intermediate by using a fusion-inhibitory peptide coupled to colloidal gold and visualized by EM. The nanobead-supported bilayers and PIV5 virions were first incubated in the presence of the C-1 peptide that binds to the prehairpin intermediate state (12). To allow gold-labeling a biotin was incorporated attached to the N terminus of the peptide via a short PEG linker. Next, streptavidin-labeled gold particles were added to label the location of the C-1 peptides and the F-protein prehairpin intermediate. The nanobead-supported bilayers, virus particles, and gold particles were then displayed by thin-sectioning and EM (Fig. 4*A*).

Approximately 300 virus/nanobead-supported bilayer images were then overlaid to show the position of the gold particles relative to the virions and nanobead-supported bilayers (Fig. 4*C*). To allow quantitative comparison of the distributions, all EM images were superimposed along a line between the center of the viral particle ellipse and the center of the PS nanobead-supported bilayers; the midpoint of the virus-nanobead vector defines the origin of the superimposed structures. The location of the gold particles relative to the virus particles and nanobead-supported bilayers are shown in red and blue circles, respectively (Fig. 4*C*). The position of the gold particles clearly localize to the contact area between the virus and the nanobead-supported bilayer (Fig. 4*A*), indicating the accumulation of F-proteins in the prehairpin intermediate state at the interface. The angle distribution of gold particles around the particles (Fig. 4*D*) supports this conclusion, and shows the particles are localized in a narrow range within 35° of the line between the centers of the two particles. The counts within this angular peak are 5 to 20-fold greater than at other angles, which represent locations outside of the contact

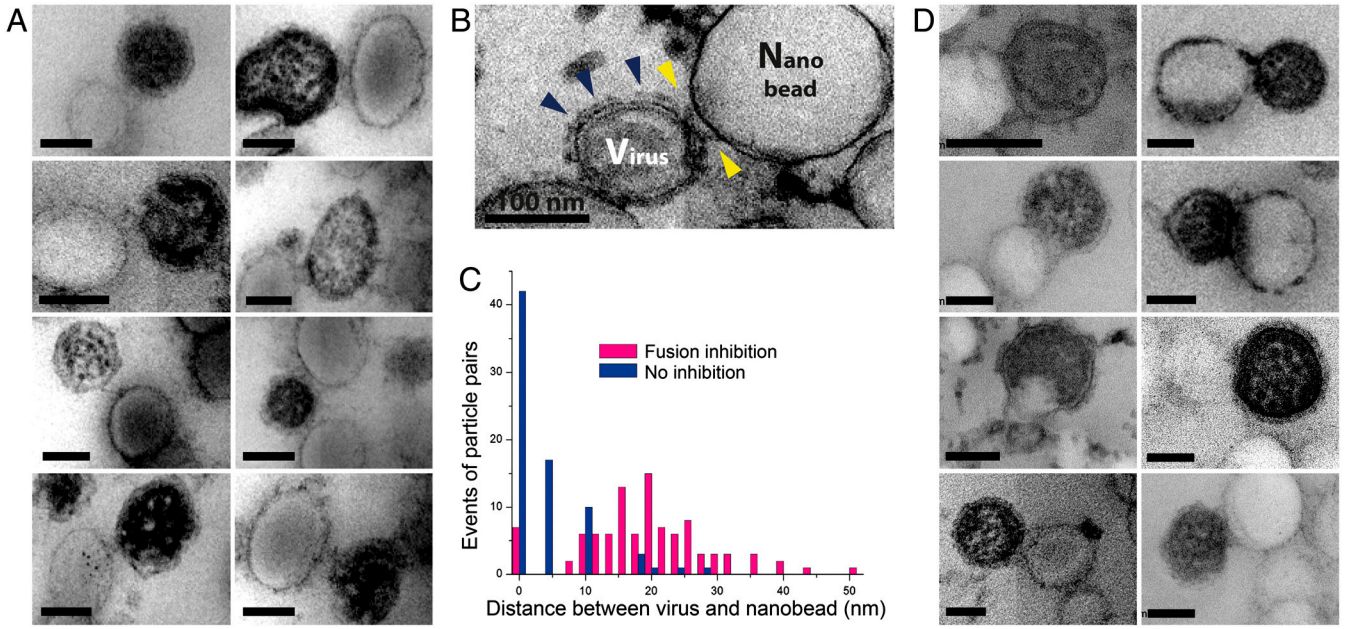

Fig. 3. Observation of the prehairpin intermediate by thin-sectioning and EM. EM gallery of viral particles and PS nanobead-supported bilayers made up of polystyrene beads from thin sectioned samples (*A*) at 42 °C in the presence of the fusion-inhibitory peptide C-1 and (*B*) in the absence of the fusion-inhibitory peptide, C-1, under the same condition as in (*A*). Under these staining conditions viral particles are darker than the PS nanobeads. (*B*) Blue arrows show the putative prefusion state in the absence of the fusion-inhibitory peptide C-1, while yellow arrows show putative prehairpin intermediates. (*C*) Distance distribution between the edge of the viral particle and nanobead with and without fusion inhibitor at 42 °C. Note the peak near 20 nm for the inhibited state. (*D*) EM gallery of viral particles fusing with nanobead-supported bilayers at 42 °C in the absence of fusion-inhibitory peptides C-1. PIV5 virions with a concentration of 1.0×10^{10} plaque forming units/mL were mixed with amino polystyrene nanobeads with a concentration of 5×10^{10} particles/mL. The faint appearance of sections in EM images is an artifact arising from four independent quadrants in the camera used for image capture.

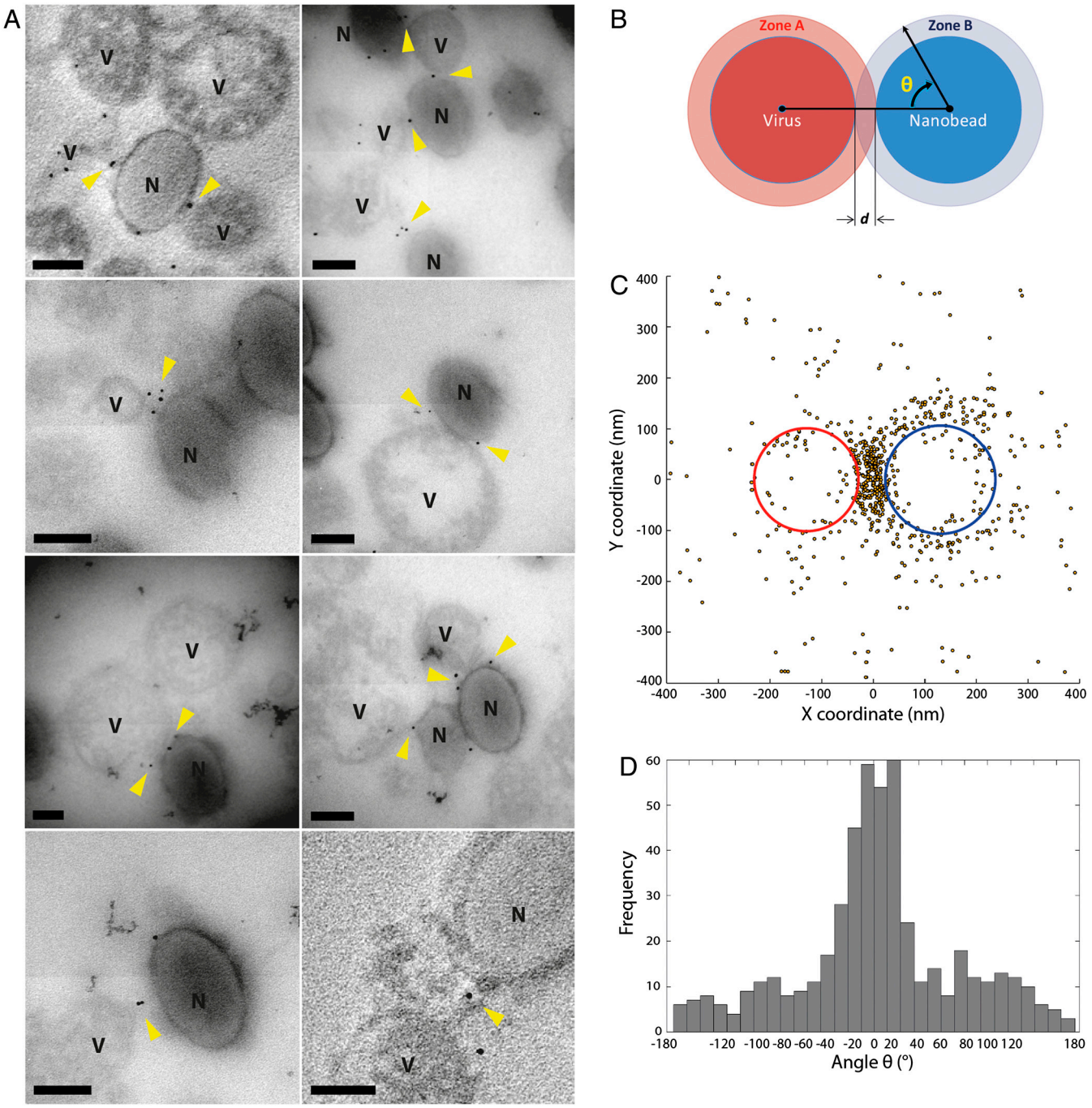

Fig. 4. Immuno-gold labeling of the fusion inhibitor shows it is concentrated between the viral particles and nanobead-supported bilayers in the trapped state. (*A*) Gallery of thin sectioned EM images of viral particles and nanobead-supported bilayers labeled using immuno-gold. The small black spheres are 5 nm gold particles. "V" labels viral particles, and "N" labels nanobeads. The thin sections containing immune-gold are approximately 70 nm thick, and produced a silver interference color. (*B*) Illustration of how the angle θ is calculated for a virus and nanobead pair. (*C*) Superimposition of the positions of all gold particles around interacting viral particles and nanobead-supported bilayers. The average virus ellipse is in red and the average nanobead-supported bilayer ellipse is in blue. Gold particles are shown as yellow dark circles. (*D*) The distribution of the angle θ. Note the large peak at 0° the angle at which a gold particle is in the space between the virus and the nanobead-supported bilayer. All scale bars in (*A*) are 100 nm. The faint appearance of sections in EM images is an artifact arising from four independent quadrants in the camera used for image capture.

zone. Thus, the prehairpin conformation segregates within the contact zone, consistent with previous findings that formation of this intermediate is triggered by contact between the virus and the target at permissive temperatures.

Conclusions

Here we confirm the existence of the viral fusion prehairpin intermediate and provide direct images of the bilayer spacing and distribution of the population of F-protein in this intermediate state. Previous evidence for the existence of the prehairpin intermediate in this and other viruses has been indirect. For example, peptides with the sequence of HRB strongly inhibit fusion despite the occlusion of its postfusion binding partner, HRA, in the prefusion state (12–14). While this result is consistent with an extended prehairpin intermediate that exposes HRA during the fusion pathway, the direct measurements made here provide strong new support for this hypothesis. Combined with computa-

tional modeling, these images also bring us much closer to an atomic level structure that could be used in the design of future entry inhibitors.

Materials and Methods

Computational Modeling of the Prehairpin Intermediate. Computational modeling of the prehairpin intermediate involved primarily four steps. First, the crystal structures of the F prefusion state of PIV5 and F postfusion states of hPIV3 were structurally aligned to create an extended model that contains both HRA and HRB as trimeric coiled coils. Second, the hPIV3 sequence was replaced by that of PIV5 and repacked. Third, the TM and fusion peptide domains were added to the model. Finally, the combined model was minimized to remove clashes.

To estimate the interbilayer spacing of the prehairpin intermediate we built a detailed atomic model of this structure (24, 25), in which the N-terminal region (residues 103–289) has extended into a trimeric coiled coil projecting towards the target bilayer, and the C-terminal residue (residues 358–511) undergoes its conformational change primarily at the late stages of fusion (going from the prehairpin intermediate to the postfusion states). This hypothesis is consistent with the fusion peptide from the N-terminal region inserting during the early stages of fusion, prior to the zippering of HRB that helps bring the bilayers together. The crystal structures of the prefusion (7) and postfusion (8) states were aligned using a region of the globular head domain, residues 290–357 (PIV5 numbering). This region is largely constant within each chain between the two structures (Cα rmsd = 1.7 Å when comparing individual chains) and presumably is also constrained in the prehairpin intermediate. While the rmsd is larger when all chains are considered because of relative rotation of the chains (Cα rmsd = 4.4 Å), a structural alignment of Cα positions places residues 357 of the postfusion structure and 358 of the prefusion structure within close proximity, allowing connection of the two regions. Therefore, the N-terminal region was taken from the postfusion structure, and the C-terminal region taken from the prefusion structure.

Second, the sequence of PIV5 was threaded onto the postfusion structure using the Rosetta Design software package to repack the new side chains (26). Repacking occurred using the default parameters. Third, for the TM domain adjacent to HRB, the model was taken from that obtained from disulfide cross linking (27). For the fusion peptide adjacent to HRA, sequence conservation data (28) supports a coiled coil structure. The coiled coil from HRA was extended into the fusion peptide to model this region, placing the most conserved residues at the core of the coiled coil. The structure was then briefly minimized (200 steps of steepest decent) in Gromacs (29) using the all-atom OPLS force field (30, 31) to relax any steric clashes in the new structure. Minimization using other force fields, such as CHARMM (32), gave very similar results.

Preparation of Nanobead-Supported Bilayers. Small unilamellar vesicles (SUVs) containing a 4:4:2 molar ratio of 1-palmitoyl-2-oleyl-*sn*-glycero-3-phosphocholine (POPC), 1,2-dioleoyl-*sn*-glycero-3-[phosphor-L-serine] (DOPC) and cholesterol (Avanti Polar Lipids) doped with 1 M% bovine brain disialoganglioside GD_{1a} (Sigma Aldrich) at a lipid concentration of 5 mM were prepared by tip sonication of vacuum dried lipid films in PBS buffer (pH 7.5, 100 mM NaCl) for 30 min. PEG-tethered silica nanobeads were prepared by the reaction of spherical bare silicas with $(C_2H_5O)_3Si(CH_2)_3O[OCH_2CH_2]_{8-12}$-OH (Gelest) in water (33). The silica particles were synthesized by Stöber's method (34). The mean particle diameter ~120 nm was assessed by EM and its surface area was determined by BET method (35). Overnight incubation of SUVs with silica and polystyrene nanobeads formed lipid-bilayers on the hydrophilic surface of silica and polystyrene nanobeads. Silica nanobeads were treated with lipid concentrations sufficient to provide coverage of ~2.5 lipids/nm^2 of the silica surfaces, which corresponds to a bilayer. Coverage was confirmed by adsorption isotherms (33), and verified by phosphorus analysis and fluorescence of NBD-doped lipids. Polystyrene nanobeads (Polyscience, amino PSs used with 5.68×10^{12} particles/mL in concentration) combined with 1 mL of 5 mM SUV stock solution formed lipid-bilayers on the hydrophilic surface of nanobeads. After encapsulation by bilayers, the silica nanobeads were rinsed at least three times with PBS buffer followed by vortexing and centrifugation at 10,000 rpm for 2 min and the supernatant was discarded. The resulting lipid-coated nanobeads were reconstituted in PBS buffer (pH 7.5). Additional sonication of the lipid-coated nanobeads was avoided so as to not disrupt the nanobead lipid bilayer. Silica nanobeads with a mean diameter of 120 nm were used. Each tube of lipid-coated silica nanobeads contains 2.8 mg of 120 nm silica nanobeads in PBS buffer. Nanobeads were vortexed or sonicated until a homogeneous suspension formed. PS nanobeads were used for the advanced EM measurements of the interparticle distance. Organic beads such as PS provide excellent contrast levels and better brightness to highlight proteins in EM. In addition, the softness of PS provides allows sectioning. For the EM measurements, aqueous suspensions were stained using 2% uranyl acetate (20) and observed using a 80 kV FEI-Tecnai T12 to display the lipid membrane on the nanobeads.

Production and Purification of PIV5 Virions. PIV5 was grown in Madin-Darby bovine kidney cells as described previously (36, 37). Virus was purified essentially as described (38) on 15–60% sucrose/NTE (100 mM NaCl, 10 mM Tris pH 7.4 and 1 mM EDTA) gradients by ultracentrifugation (24,000 rpm for 2 h at 4 °C) in a Beckman SW 32 rotor. The virus band was collected, diluted in NTE buffer, and virus pelleted at 100,000 × *g* for 1 h in a Beckman Ti60 rotor. The viral pellet was resuspended in NTE buffer and Dounce homogenized. Purified PIV5 virions were aliquoted in with a concentration of 1.0×10^{10} plaque forming units (PFU) per mL and stored at −80 °C.

Electron Microscopy in Combination with Sectioning and Staining Techniques.
Electron microscopy. EM images were taken on a JEOL 2010 microscope operating at 120 kV or 200 kV for sectioned samples and a FEI-Tecnai G12 operating at 80 kV for silica nanobead-coated bilayers. The imaging device was a Gatan image filter, and the Gatan Digital Micrograph software was used to record the images. In the case of lipid-coated silica nanobeads (Fig. 2), droplets of an aqueous suspension of a mixture of silica nanobead-supported bilayers and PIV5 viruses were dropcast onto a carbon grid (Electron Microscopy Sciences, 400-mesh) and visualized on an FEI-Tecnai G12 Transmission electron microscope at 80 kV.

Negative/positive staining and sectioning protocols. The standard process of sample fixation with paraformaldehyde or glutaraldehyde caused artifacts in the EM examination after sectioning and was not used. Samples were fixed in 2% osmium tetroxide (OsO_4) with 1.5% potassium ferricyanide in 0.1 M sodium cacodylate buffer for 1 h at room temperature. OsO_4 is known to stabilize many proteins by transforming them into gels without destroying structural features (39). Proteins that are stabilized by OsO_4 are not aggregated by alcohols during dehydration. After washes in dH_2O, samples were stained *en bloc* with 2% aqueous uranyl acetate (20) prior to dehydration in a graded ethanol series. Samples were embedded in a PolyBed 812 bed (Polysciences Inc.). The embedded samples were sectioned on an ultramicrotome. Thin sections were transferred to coated 300 mesh grids and were additionally stained with uranyl acetate, OsO_4, tannic acid, phosphotungstic acid (PTA), and bismuth subnitrite (40). Staining times varied from 5 min to 30 min.

Optimizing contrast of proteins and membranes against other compartments in PIV5 virus. The sectioning and staining protocols were optimized to increase the visibility of proteins on the viral surface (Fig. S2). OsO_4 embeds into membranes, creating a high secondary electron emission without the need for coating the membrane with a layer of metal which could obscure details of the cell membrane (41). In staining the viral surface spike proteins (F and HN), tannic acid-UA is commonly used as both a negative and positive stain to improve resolution (42). The positively stained EM presents protein compartments and nucleocapsids when combined with tannic acid and UA, thus creating contrast. Depending on the presence of immuno-gold labels, the staining conditions were found to be optimal at condition A (no immuno-gold): 1% tannic acid (30 min)/2% UA(30 min) (Fig. 3 *A* and *D*) or condition B (with immuno-gold): 2% OsO_4 (30 min)/1% tannic acid(30 min)/2% UA(10 min) (Fig. 3*B*).

Synthesis and Purification of Inhibitory Fusion Peptide. Previous studies have demonstrated that the inhibitory peptide C-1, derived from the heptad repeat region B (HRB) of PIV5 F-protein, displays antiviral activity (43). The sequence is: KLESSQILSIDPLDISQNLAAVNKSLSDALQHLAQSDTYLSAI. The C-1 was synthesized by solid-phase synthesis using Fmoc chemistry with HBTU (O-benzotriazole-N,N,N′,N′-tetramethyl-uronium-hexafluoro-phosphate) as a coupling agent; biotin was attached via a flexible linker by coupling first Fmoc-8-amino-3,6-dioxaoctanoic acid (PEPTIDES Internationals) then a single cysteine residue to biotin (5-[(3aS,4S,6aR)-2-oxohexahydro-1*H*-thieno [3,4-*d*] imidazol-4-yl] pentanoic acid, Sigma-Aldrich). The products were cleaved from the rink amide MBHA resin (Novabiochem, substitution level of 0.56 mmole/g) in a mixture of trifluoroacetic acid (TFA)/triisopropyl silane/H_2O (95:2.5:2.5 vol/vol) at room temperature under N_2 flow for 2 h. The crude peptides, precipitated with cold diethyl ether (Aldrich), were dried in vacuo. Purification proceeded by preparative reverse phase high performance liquid chromatography (HPLC, Varian ProStar 210) using a preparative C4 column (Vydac) and a linear gradient of buffer A (99.9% H_2O and 0.1% trifluoroacetic acid) and buffer B (90% acetonitrile, 9.9% H_2O and 0.1%

trifluoroacetic acid). Purity was assessed using an HP1100 analytical HPLC system (Hewlett Packard) with a C4 column (Vydac). Molecular mass of all peptides was confirmed by matrix-assisted laser desorption/ionization-time of flight (MALDI-TOF) mass spectrometry using a Bruker Microflex 3.1.

Immuno-Gold Assay for Tracking the Prehairpin Intermediate State. Immunogold labeling EM was performed using a JEOL 2010 microscope operated at an acceleration voltage of 120 kV. The PIV5 virus particles were incubated with lipid-coated PS nanobeads at 42 °C in the presence of biotinylated C-1 peptide using varied incubation time from 2 min to 1 h, followed by incubation with streptavidin-coated 5 nm gold particles (Ted Pella) for 10 min. The posttreatment with 5 nm gold particles labels the inhibitory peptide to show the location of the inhibited fusion proteins. The same thin-sectioning protocols were followed as in the other fusion assay. In the case of the gold labels, the staining protocol allows for higher contrast against the light membrane of the viruses and nanobeads.

Angular Distribution of Gold Particle Binding to Fusion Proteins in Immuno-Gold Assay. For the localization of the prehairpin intermediate, EM images of viral particle/PS nanobead pairs including immuno-gold were analyzed using a JEOL 2010 microscope with over 200 images (about 300 pairs) in five sectioned samples. In order to present a full distribution of gold particles binding to fusion protein in PIV5 virus, all EM images were superimposed such that the midpoint of the line between the center of the viral particle ellipse and the center of the PS nanobead-supported bilayers ellipse are at the origin, the viral particle is on the negative *x* axis, and the nanobead-supported bilayer is on the positive *x* axis (Fig. 4*C*). The alignments were made using the Matlab computing language. The angles of gold particles within 200 nm of the nanobead-supported bilayer center were then quantified (Fig. 4*D*).

ACKNOWLEDGMENTS. We thank Dong Kuyn Ko and Taejong Baik for EM measurements. We also thank Raymond Meade and Biao Zuo in BioMedical Imaging Core at University of Pennsylvania for preparation of all sectioned and stained samples for EM analysis. This work was supported by National Institutes of Health (NIH) grants (GM54616, AI-23173) and the Materials Research Science and Engineering Centers (MRSEC) program of the National Science Foundation (NSF). G.P.L. is a Research Specialist and R.A.L. is an Investigator of the Howard Hughes Medical Institute.

1. Harrison SC (2008) Viral membrane fusion. *Nat Struct Mol Biol* 15:690–698.
2. Lamb RA, Jardetzky TS (2007) Structural basis of viral invasion: lessons from paramyxovirus F. *Curr Opin Struct Biol* 17:427–436.
3. Colman PM, Lawrence MC (2003) The structural biology of type I viral membrane fusion. *Nat Rev Mol Cell Biol* 4:309–319.
4. Weissenhorn W, et al. (1999) Structural basis for membrane fusion by enveloped viruses. *Mol Membr Biol* 16:3–9.
5. Cross KJ, Burleigh LM, Steinhauer DA (2001) Mechanisms of cell entry by influenza virus. *Expert Reviews in Molecular Medicine* 3:1–18.
6. White JM, Delos SE, Brecher M, Schornberg K (2008) Structures and mechanisms of viral membrane fusion proteins: multiple variations on a common theme. *Crit Rev Biochem Mol Biol* 43:189–219.
7. Yin HS, Wen X, Paterson RG, Lamb RA, Jardetzky TS (2006) Structure of the parainfluenza virus 5 F protein in its metastable, prefusion conformation. *Nature* 439:38–44.
8. Yin HS, Paterson RG, Wen X, Lamb RA, Jardetzky TS (2005) Structure of the uncleaved ectodomain of the paramyxovirus (hPIV3) fusion protein. *Proc Natl Acad Sci USA* 102:9288–9293.
9. Wilson IA, Skehel JJ, Wiley DC (1981) Structure of the haemagglutinin membrane glycoprotein of influenza virus at 3 A resolution. *Nature* 289:366–373.
10. Bullough PA, Hughson FM, Skehel JJ, Wiley DC (1994) Structure of influenza haemagglutinin at the pH of membrane fusion. *Nature* 371:37–43.
11. Brunner J, Zugliani C, Mischler R (1991) Fusion activity of influenza virus PR8/34 correlates with a temperature-induced conformational change within the hemagglutinin ectodomain detected by photochemical labeling. *Biochemistry* 30:2432–2438.
12. Russell CJ, Jardetzky TS, Lamb RA (2001) Membrane fusion machines of paramyxoviruses: capture of intermediates of fusion. *EMBO J* 20:4024–4034.
13. Chan DC, Kim PS (1998) HIV entry and its inhibition. *Cell* 93:681–684.
14. Jiang S, Lin K, Strick N, Neurath AR (1993) HIV-1 inhibition by a peptide. *Nature* 365:113.
15. Lee KK (2010) Architecture of a nascent viral fusion pore. *EMBO J* 29:1299–1311.
16. Damico RL, Crane J, Bates P (1998) Receptor-triggered membrane association of a model retroviral glycoprotein. *Proc Natl Acad Sci USA* 95:2580–2585.
17. Furuta RA, Wild CT, Weng Y, Weiss CD (1998) Capture of an early fusion-active conformation of HIV-1 gp41. *Nat Struct Biol* 5:276–279.
18. Tanaka M, Sackmann E (2005) Polymer-supported membranes as models of the cell surface. *Nature* 437:656–663.
19. Baker KA, Dutch RE, Lamb RA, Jardetzky TS (1999) Structural basis for paramyxovirus-mediated membrane fusion. *Mol Cell* 3:309–319.
20. Yuan P, et al. (2005) Structural studies of the parainfluenza virus 5 hemagglutinin-neuraminidase tetramer in complex with its receptor, sialyllactose. *Structure* 13:803–815.
21. Crennell S, Takimoto T, Portner A, Taylor G (2000) Crystal structure of the multifunctional paramyxovirus hemagglutinin-neuraminidase. *Nat Struct Biol* 7:1068–1074.
22. Lamb RA, Parks GD (2007) *Fields Virology*, eds DM Knipe and PM Howley, pp 1449–1496.
23. Paterson RG, Russell CJ, Lamb RA (2000) Fusion protein of the paramyxovirus SV5: destabilizing and stabilizing mutants of fusion activation. *Virology* 270:17–30.
24. Lamb RA (1993) Paramyxovirus fusion: a hypothesis for changes. *Virology* 197:1–11.
25. Carr CM, Kim PS (1993) A spring-loaded mechanism for the conformational change of influenza hemagglutinin. *Cell* 73:823–832.
26. Rohl CA, Strauss CE, Misura KM, Baker D (2004) Protein structure prediction using Rosetta. *Methods Enzymol* 383:66–93.
27. Bissonnette ML, Donald JE, DeGrado WF, Jardetzky TS, Lamb RA (2009) Functional analysis of the transmembrane domain in paramyxovirus F protein-mediated membrane fusion. *J Mol Biol* 386:14–36.
28. Donald JE, et al. From the cover: transmembrane orientation and possible role of the fusogenic peptide from parainfluenza virus 5 (PIV5) in promoting fusion. *Proc Natl Acad Sci USA* 108:3958–3963.
29. Van Der Spoel D, et al. (2005) GROMACS: fast, flexible, and free. *J Comput Chem* 26:1701–1718.
30. Jorgensen WL, Maxwell DS, Tirado-Rives J (1996) Development and testing of the OPLS all-atom force field on conformational energetics and properties of organic liquids. *J Am Chem Soc* 118:11225–11236.
31. Kaminski GA, Friesner RA, Tirado-Rives J, Jorgensen WL (2001) Evaluation and reparametrization of the OPLS-AA force field for proteins via comparison with accurate quantum chemical calculations on peptides. *J Phys Chem B* 105:6474–6487.
32. MacKerell AD, Jr, et al. (1998) All-atom empirical potential for molecular modeling and dynamics studies of proteins. *J Phys Chem B* 102:3586–3616.
33. Fadeev AY, DeGrado WF (2011) Lipid membranes supported on optically transparent nanosilicas: synthesis and application in characterization of protein-membrane interactions. *J Colloid Interface Sci* 355:265–268.
34. Stöber W, Fink A, Bohn E (1968) Controlled growth of monodisperse silica spheres in the micron size range. *J Colloid Interf Sci* 26:62–69.
35. Gregg SJ, Sing KSW (1982) *Adsorption, Surface Area, and Porosity* (Academic Press, London).
36. Peluso RW, Lamb RA, Choppin PW (1977) Polypeptide synthesis in simian virus 5-infected cells. *J Virol* 23:177–187.
37. Paterson RG, Harris TJ, Lamb RA (1984) Analysis and gene assignment of mRNAs of a paramyxovirus, simian virus 5. *Virology* 138:310–323.
38. Lamb RA, Mahy BW, Choppin PW (1976) The synthesis of sendai virus polypeptides in infected cells. *Virology* 69:116–131.
39. Hayat MA (2000) *Principles and Techniques of Electron Microscopy: Biological Applications* (Cambridge University Press, Cambridge United Kingdom; New York).
40. Yamaguchi K, Suzuki K, Tanaka K (2010) Examination of electron stains as a substitute for uranyl acetate for the ultrathin sections of bacterial cells. *J Electron Microsc (Tokyo)* 59:113–118.
41. Bozzola JJ, Russell LD (1999) *Electron Microscopy: Principles and Techniques for Biologists* (Jones and Bartlett, Sudbury, Mass).
42. Haidar A, Ryder TA, Mobberley MA, Wigglesworth JS (1992) Two techniques for electron opaque staining of elastic fibres using tannic acid in fresh and formalin fixed tissue. *J Clin Pathol* 45:633–635.
43. Joshi SB, Dutch RE, Lamb RA (1998) A core trimer of the paramyxovirus fusion protein: parallels to influenza virus hemagglutinin and HIV-1 gp41. *Virology* 248:20–34.

LETTER

doi:10.1038/nature10718

T-cell differentiation factor CBF-β regulates HIV-1 Vif-mediated evasion of host restriction

Wenyan Zhang[1]*, Juan Du[1,2]*, Sean L. Evans[2], Yunkai Yu[2] & Xiao-Fang Yu[1,2]

The human APOBEC3 cytidine deaminases are potent inhibitors of diverse retroviruses, including human immunodeficiency virus-1 (HIV-1)[1–6]. HIV-1 Vif forms an E3 ubiquitin ligase complex with cullin 5 (CUL5), elongin B and elongin C [7–9], which promotes the polyubiquitination and degradation of APOBEC3 substrates[7,10–14]. Here we demonstrate in human T cells that core binding factor β (CBF-β) is a key regulator of the evasion of HIV-1 from the host defence mediated by APOBEC3. CBF-β, the non-DNA-binding subunit of a heterodimeric transcription factor, regulates the folding and DNA-binding activity of partner RUNX family proteins, which have important roles in the development and differentiation of diverse cell types, including T lymphocytes[15,16]. In our study, knockdown of endogenous CBF-β blocked Vif-induced APOBEC3G polyubiquitination and degradation. CBF-β was not required for the interaction between Vif and APOBEC3G, yet was essential for the assembly of the Vif–CUL5 E3-ubiquitin-ligase complex. CBF-β proved to be a unique regulator of primate lentiviral Vif and not a general component of the CUL5 E3 ubiquitin ligase. We show that Vif and CBF-β physically interact, and that the amino-terminal region of Vif is required for this interaction. Furthermore, interactions with Vif required regions in CBF-β that are not involved in RUNX protein binding[17–19]. Considering the importance of the interaction between Vif and CBF-β, disrupting this interaction represents an attractive pharmacological intervention against HIV-1.

To identify novel cellular proteins involved in HIV-1 Vif function, we infected human $CD4^+$ T cells (H9) with HIV-1 Vif–haemagglutinin (HA) or HIV-1 (control) virus[7] and then characterized the interaction of cellular proteins with HIV-1 Vif–HA in the infected cells by co-immunoprecipitation analysis. HIV-1 Vif forms an E3 ubiquitin ligase with CUL5 and elongin B/elongin C (ELOB/C) to promote the polyubiquitination and degradation of various substrates, including APOBEC3 and Vif itself[8,20]. To limit the potential degradation of these co-factors, we treated the cells with the proteasome inhibitor MG132 before co-immunoprecipitation. HA-tagged Vif was immunoprecipitated with anti-HA antibody from HIV-1 Vif–HA-infected H9 cell lysates but not HIV-1 (control)-infected H9 cell lysates (Fig. 1a). Immunoprecipitation of Vif–HA was confirmed by immunoblotting with a HA-specific antibody (Fig. 1b). Untagged Vif was not immunoprecipitated from control-infected H9 cells (Fig. 1b, lane 2). CUL5 (84 kDa) was co-precipitated with Vif–HA (Fig. 1a, lane 1) and confirmed by immunoblotting with a CUL5-specific antibody (Fig. 1b, lane 1); ELOB/C was also co-precipitated with Vif–HA (Fig. 1b, lane 1). These proteins were not co-precipitated from control HIV-1-infected H9 cells (Fig. 1b, lane 2).

A previously uncharacterized protein of ~22 kDa also co-precipitated with Vif–HA (Fig. 1a, lane 1). This protein was identified by mass spectrometry analysis as CBF-β, a ubiquitously expressed host protein[15,16]. The identification of the protein was confirmed by immunoblotting with a CBF-β-specific antibody (Fig. 1b, lane 1). We also detected an interaction between HIV-1 Vif–HA and CBF-β in transfected 293T (human embryonic kidney) cells (Fig. 1c, lane 4), indicating that the interaction between CBF-β and HIV-1 Vif can occur in the absence of

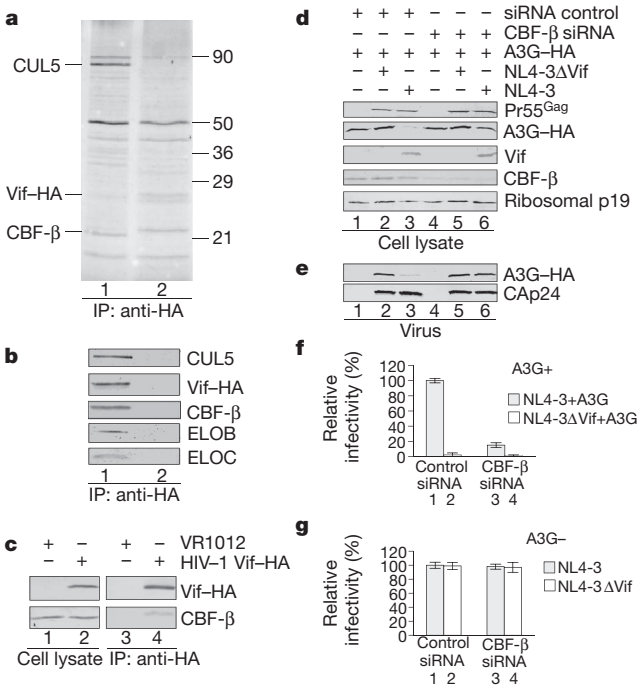

Figure 1 | Characterization of the functional interaction between HIV-1 Vif and CBF-β. a, Co-immunoprecipitation of cellular proteins with Vif–HA. Cell lysates from H9 cells infected with HIV-1 Vif–HA (HXB2Neo-Vif-HA, lane 1) or with control HIV-1 (that is, HXB2Neo containing untagged Vif, lane 2) were immunoprecipitated (IP) with anti-HA antibody conjugated to agarose beads, followed by SDS–PAGE and silver staining. The identification of CBF-β co-precipitated with Vif–HA (lane 1) was achieved by mass spectrometry. **b**, Immunoblot of precipitated samples from HIV-1- or HIV-1 Vif–HA-infected H9 cells using antibodies against CUL5, CBF-β, ELOB, ELOC or HA (to detect Vif–HA). **c**, Co-immunoprecipitation of endogenous CBF-β with Vif–HA from transfected 293T-cell samples. **d**, Vif-mediated downregulation of APOBEC3G (A3G) requires CBF-β. 293T cells were co-transfected with expression vectors for APOBEC3G–HA plus NL4-3, NL4-3ΔVif, or a control vector (pcDNA3.1) in the presence of control siRNA (lanes 1–3) or siRNA against CBF-β (lanes 4–6). **e**, CBF-β is required for Vif-mediated exclusion of APOBEC3G from virions. **e**, **f**, Supernatants from transfected 293T cells as described in **d** were collected and analysed for APOBEC3G–HA virion packaging (**e**) and viral infectivity (**f**). **f**, Virus infectivity was assessed by multinuclear activation of a galactosidase indicator (MAGI) assay. Virus input was normalized by the amount of CAp24. Virus infectivity with NL4-3 (Vif-positive) produced from transfected 293T cells in the presence of control siRNA was set to 100%. Error bars in **f** and **g** represent the standard deviations from triplicate wells. **g**, Silencing CBF-β expression had no effect on viral infectivity in the absence of APOBEC3G.

[1]First Hospital of Jilin University, Institute of Virology and AIDS Research, Changchun, Jilin Province 130021, China. [2]Department of Molecular Microbiology and Immunology, Johns Hopkins Bloomberg School of Public Health, 615 N. Wolfe Street, Baltimore, Maryland 21205, USA.
*These authors contributed equally to this work.

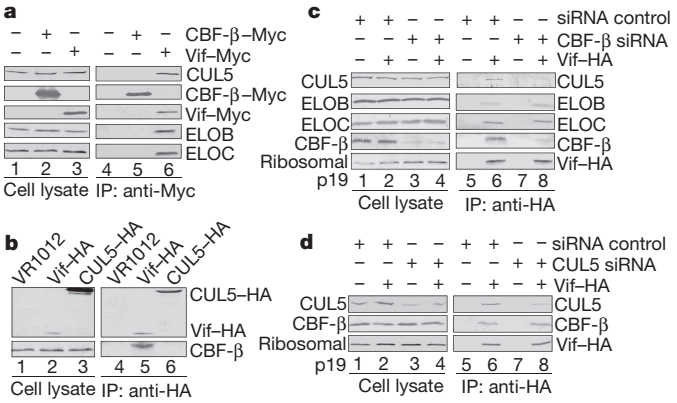

Figure 2 | CBF-β is critical for the interaction between Vif and CUL5. **a**–**d**, 293T cells were transfected with the indicated expression vectors. Cell lysates were prepared and immunoprecipitated followed by immunoblot analysis as described in Fig. 1. **a**, Co- immunoprecipitation of CUL5, ELOB and ELOC with Vif–Myc but not CBF-β–Myc. **b**, Co-immunoprecipitation of endogenous CBF-β with Vif–HA but not CUL5–HA. **c**, Silencing CBF-β inhibits the interaction between Vif and CUL5. **d**, Silencing CUL5 does not affect the Vif–CBF-β interaction.

other viral proteins. MG132 treatment increased the stability of HIV-1 Vif but did not alter its interaction with CBF-β (Supplementary Fig. 1); RNase treatment also did not block its interaction with CBF-β. Using a live cell imaging approach, we observed co-localization of yellow fluorescent protein (YFP)–Vif and cyan fluorescent protein (CFP)–CBF-β in transfected 293T cells along with a positive fluorescence resonance energy transfer (FRET) signal, further validating a physical interaction (Supplementary Fig. 2).

To determine whether CBF-β is required for the function of HIV-1 Vif, we knocked down endogenous CBF-β expression by CBF-β-specific short interfering RNA (siRNA). As compared to control siRNA-treated cells (Fig. 1d, lanes 1–3), CBF-β was reduced by ~70% in 293T cells treated with CBF-β-specific siRNA (lanes 4–6). In the control siRNA-treated cells, HIV-1 Vif efficiently reduced the expression of APOBEC3G (lane 3) when compared to HIV-1 NL4-3 strain Vif-negative (NL4-3ΔVif) virus-expressing cells (lane 2). Silencing of endogenous CBF-β (lanes 4–6) impeded the ability of Vif to reduce the expression of APOBEC3G (lane 6). Because HIV-1 Vif mainly reduces the expression of APOBEC3G by inducing its degradation, these data indicated that CBF-β is required for the HIV-1 Vif-mediated degradation of APOBEC3G (Fig. 1d, compare lanes 2 and 3 to lanes 5 and 6). Interestingly, expression of exogenous CFP–CBF-β enhanced both wild-type, untagged Vif (pcDNA-hVif)- and YFP–Vif-induced APOBEC3G degradation in 293T cells (Supplementary Fig. 2).

To exert its antiviral activity, APOBEC3G must be packaged into HIV-1 virions so that it can then inhibit virus infectivity in new target cells; Vif suppresses this antiviral activity by limiting the packaging of APOBEC3G into virions. Indeed, we found that when Vif was present, APOBEC3G was efficiently excluded from released HIV-1 virions in control siRNA-treated cells (Fig. 1e, lane 3); when Vif was absent, APOBEC3G could be packaged into HIV-1 virions (Fig. 1e, lane 2). However, the ability of Vif to exclude APOBEC3G from released HIV-1 virions was markedly compromised when CBF-β expression was knocked down in virus-producing cells (Fig. 1e, compare lanes 3 and 6). Reducing the expression of CBF-β specifically blocked the ability of HIV-1 Vif to suppress the antiviral activity of APOBEC3G (Fig. 1f). In contrast, silencing CBF-β expression had no effect on the viral infectivity of NL4-3 or NL4-3ΔVif when APOBEC3G was absent (Fig. 1g), indicating that CBF-β regulates HIV-1 infectivity only in the presence of APOBEC3G.

CBF-β apparently does not interact directly with APOBEC3G and is not required for the Vif–APOBEC3G interaction (Supplementary Fig. 3). Human APOBEC3F is another human cytidine deaminase that has potent anti-HIV-1 activity; however, APOBEC3F and APOBEC3G are recognized by HIV-1 Vif through distinct mechanisms[21–27]. We postulated that if CBF-β is not involved in Vif-substrate recognition, it most likely regulates Vif mediated suppression of APOBEC3F as well as APOBEC3G. Indeed, HIV-1 Vif-mediated degradation, virion exclusion and suppression of APOBEC3F also required CBF-β (Supplementary Fig. 4). Thus, CBF-β is apparently required for Vif activity at a critical step(s) other than substrate recognition.

Because CBF-β does not affect the interaction between HIV-1 Vif and APOBEC3G, it is possible that CBF-β influences the ubiquitin ligase activity of Vif–CUL5 E3 and could in fact be a previously unrecognized component of the CUL5–ELOB/C E3 ubiquitin ligase. To determine whether CBF-β is an integral component of this complex, we examined the interaction of CBF-β with CUL5 and ELOB/C. Co-immunoprecipitation of CUL5 and ELOB/C with HIV-1 Vif–Myc (Fig. 2a, lane 6) was readily detected, but there was no co-immunoprecipitation of CUL5 or ELOB/C with CBF-β–Myc under the same conditions (lane 5). We also saw no interaction between endogenous CBF-β and CUL5–HA in a reciprocal co-immunoprecipitation analysis (Fig. 2b, lane 6), despite a readily detectable interaction between CBF-β and Vif–HA (lane 5). Therefore, CBF-β is unlikely to be an integral component of the CUL5–ELOB/C E3 complex under physiological conditions.

To determine whether CBF-β might have a role in the assembly of the Vif–CUL5 E3 ubiquitin ligase, we examined the interaction of Vif–HA with endogenous CUL5 and ELOB/C by co-immunoprecipitation analysis. Reducing CBF-β expression with specific siRNA had no effect on the intracellular expression of CUL5 or ELOB/C (Fig. 2c, compare lanes 1 and 2 to lanes 3 and 4). CUL5 and ELOB/C were co-immunoprecipitated with HIV-1 Vif–HA by the anti-HA antibody in control siRNA-treated cells (lane 6), but not in control cells that did not express HIV-1 Vif–HA (lanes 5 and 7). Co-immunoprecipitation of CUL5 with HIV-1 Vif–HA was significantly inhibited when CBF-β was silenced (Fig. 2c, lane 8) but co-precipitation of ELOB/C with HIV-1 Vif–HA was not (lane 8). Although silencing of CBF-β inhibited the interaction of Vif with CUL5 (Fig. 2c), reciprocal silencing of CUL5 (Fig. 2d, lane 4) had no

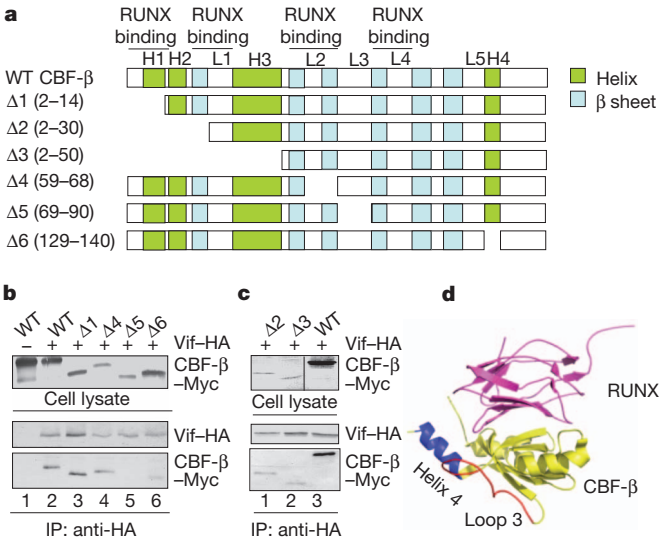

Figure 3 | Identification of regions in CBF-β is important for HIV-1 Vif interaction. **a**, Diagrams of mutant CBF-β constructs. The numbers in parentheses indicate amino acids that were deleted in the mutant CBF-β constructs. **b**, **c**, Co-precipitation of full-length (wild-type; WT) CBF-β–Myc and CBF-β mutants with HIV-1 Vif–HA. Cell lysates and precipitated samples were analysed by immunoblotting with an anti-Myc or anti-HA antibody. **d**, The structures of CBF-β (yellow) complexed with RUNX1 (pink) have been well characterized[17–19]. Loop 3 (red) and helix 4 (blue) of CBF-β, which are located away from the interfaces between CBF-β and RUNX1, are important for the Vif–CBF-β interaction.

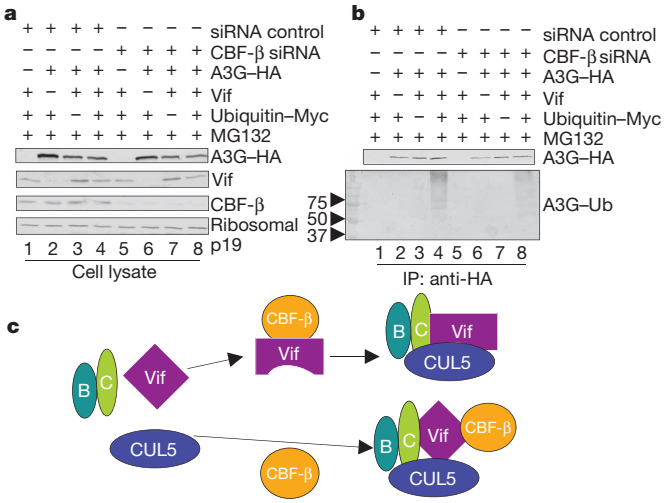

Figure 4 | Vif-induced polyubiquitination of APOBEC3G requires CBF-β. **a**–**c**, 293T cells were transfected with an expression vector encoding APOBEC3G–HA (A3G–HA), Vif, Myc-tagged ubiquitin (Ub) or control vector as indicated. All experiments were performed in the presence of MG132. **a**, Cells were lysed and analysed by immunoblot analysis using an anti-Vif, anti-CBF-β or anti-HA antibody. **b**, Cell lysates were immunoprecipitated with the anti-HA antibody and analysed by immunoblotting with an anti-Myc antibody to detect ubiquitinated APOBEC3G. Unmodified APOBEC3G–HA was detected with the anti-HA antibody. **c**, Proposed models for the role of CBF-β in HIV-1 Vif function.

detectable effect on the CBF-β–Vif interaction (Fig. 2d, lane 8). Again, these data indicate that CBF-β is not a general co-factor of CUL5, and CBF-β uniquely regulates the interaction of HIV-1 Vif with CUL5.

We also observed that the activity of the adenoviral E4orf6-containing CUL5–ELOB/C ubiquitin ligase was not affected by CBF-β silencing (Supplementary Fig. 5). In addition, cellular SOCS-box-containing proteins (that is, ASB6 and SOCS3) (Supplementary Fig. 5), which are known to assemble with the CUL5–ELOB/C E3 ubiquitin ligase, did not interact with CBF-β. Also, although primate lentiviral Vif interacted with CBF-β, Vif from bovine immunodeficiency virus (BIV) did not (Supplementary Fig. 6). BIV Vif-mediated bovine APOBEC3 depletion was not affected by CBF-β silencing.

CBF-β is a ubiquitously expressed component of a heterodimeric transcription factor including RUNX family proteins[15,16]. The interface between CBF-β and RUNX proteins is well defined[17–19]. To explore the regions of CBF-β and HIV-1 Vif that are critical for their interaction, we first examined the Vif-binding activity of a series of in-frame CBF-β deletion mutants (Fig. 3a). The regions of CBF-β that were important for the interaction with HIV-1 Vif mapped to loop 3 and helix 4 (Fig. 3b, c), regions that do not interact with RUNX proteins (Fig. 3d).

Consistent with the idea that HIV-1 Vif does not compete with RUNX for binding to CBF-β, we observed that the interaction of RUNX1 with CBF-β was not affected by the presence of Vif (Supplementary Fig. 7); in fact, a possible co-precipitation of Vif–HA with RUNX1–Myc was detected (Supplementary Fig. 7). RUNX1-mediated transcriptional activity[28] was also not significantly affected by Vif, as measured in a CBF promoter-driven luciferase reporter assay (Supplementary Fig. 7). We determined that the N-terminal regions of Vif, including amino acids W21 and W38, were important for CBF-β binding (Supplementary Fig. 8).

To determine whether CBF-β can influence the HIV-1 Vif-induced polyubiquitination of APOBEC3G, we transfected 293T cells with various combinations of expression vectors for HIV-1 Vif–Myc, APOBEC3G–HA and Myc-tagged ubiquitin in the presence of control siRNA or siRNA against CBF-β (Fig. 4a). To inhibit APOBEC3G degradation, all transfected cells were treated with MG132. HA-tagged APOBEC3G was immunoprecipitated by the anti-HA antibody, followed by the detection of ubiquitinated APOBEC3G–HA using the antibody against Myc-tagged ubiquitin. Polyubiquitinated APOBEC3G–HA was detected in cells expressing Vif (Fig. 4b, lane 4); however, the Vif-induced polyubiquitination of APOBEC3G was inhibited by siRNA against CBF-β (lane 8).

Taken together, our results demonstrate that CBF-β is a key regulator of HIV-1 Vif function. We have further shown that CBF-β is critical for Vif-induced endogenous APOBEC3G degradation and HIV-1 replication in H9 $CD4^+$ T cells (Supplementary Fig. 9). CBF-β allosterically regulates the conformation and DNA-binding activity of RUNX proteins[17–19]. It remains to be determined, however, whether CBF-β can induce conformational changes in HIV-1 Vif that allow CUL5 binding to occur. Alternatively, CBF-β may stabilize the interaction between Vif and CUL5 in the E3 ubiquitin ligase complex (Fig. 4c). Vif–CBF-β binding is critical for HIV-1 infection but does not seem to interfere with normal CBF-β–RUNX interaction. Thus, the interface between Vif and CBF-β may constitute a promising target for new anti-HIV drug discovery.

METHODS SUMMARY

Live-cell imaging and FRET assay. 293T cells were transfected with YFP–Vif (2 μg) and CFP–CBF-β (0.25 μg) using Lipofectamine 2000 (Invitrogen) in 6-well coverslip glass-bottom cell culture dishes (MatTek) at 37 °C with 5% CO_2. Eightfold excess YFP–Vif was used due to low expression of YFP–Vif compared to CFP–CBF-β (Supplementary Fig. 2d). YFP–CFP dimer (0.25 μg), co-transfection of YFP (0.25 μg) plus CFP (0.25 μg), and CFP–CBF-β alone were used for a positive and negative FRET signal as imaging controls. Cells were visualized 24–36 h after transfection using a Zeiss LSM510-Meta confocal imaging system equipped with four argon lasers (458, 477, 488 and 514 nm lines), two HeNe lasers (542 and 633 nm), and one diode laser (405 nm). YFP and CFP were excited using a 514 nm and 458 nm laser, respectively. After excitation, channel mode images were collected using a long-pass filter for CFP emission (LP 420) or band-pass filter for YFP emission (BP 530-600). In addition, the channel mode detector gain was set so that neither CFP nor YFP images contained saturated pixels before bleaching. A total of ten images (five pre-bleach and five post-bleach) were acquired for each cell with a ×63 objective with ×2 zoom, and image analysis and manipulation was performed using Zeiss LSM imaging software. FRET analysis was performed using the acceptor photo-bleaching technique: YFP or YFP–Vif was photo-bleached for approximately 5 min at 514 nm (100% laser power), and the average donor signal was evaluated before and after acceptor photobleaching. As a control, cells were also imaged under similar conditions, except the 514 nm laser was set at 0% transmission to prevent acceptor photobleaching. Two experiments were performed for each bleached sample for a total of ten cells each. One experiment was performed for each unbleached sample for a total of four cells each. The FRET efficiency percentage (E) was calculated using the FRET macro of Zeiss LSM software. The following equation was used: $E = (F_{D\Delta}/F_{Dpost}) \times 100$, where $F_{D\Delta}$ is the change in donor (CFP) fluorescence intensity before and after acceptor (YFP) bleaching and F_{Dpost} is donor fluorescence intensity after acceptor bleaching. The FRET macro of Zeiss LSM software also subtracts background when calculating E.

Full Methods and any associated references are available in the online version of the paper at www.nature.com/nature.

Received 27 May; accepted 17 November 2011.
Published online 21 December 2011.

1. Sheehy, A. M., Gaddis, N. C., Choi, J. D. & Malim, M. H. Isolation of a human gene that inhibits HIV-1 infection and is suppressed by the viral Vif protein. *Nature* **418,** 646–650 (2002).
2. Navarro, F. & Landau, N. R. Recent insights into HIV-1 Vif. *Curr. Opin. Immunol.* **16,** 477–482 (2004).
3. Cullen, B. R. Role and mechanism of action of the APOBEC3 family of antiretroviral resistance factors. *J. Virol.* **80,** 1067–1076 (2006).
4. Chiu, Y. L. & Greene, W. C. The APOBEC3 cytidine deaminases: an innate defensive network opposing exogenous retroviruses and endogenous retroelements. *Annu. Rev. Immunol.* **26,** 317–353 (2008).
5. Malim, M. H. & Emerman, M. HIV-1 accessory proteins—ensuring viral survival in a hostile environment. *Cell Host Microbe* **3,** 388–398 (2008).
6. Goila-Gaur, R. & Strebel, K. HIV-1 Vif, APOBEC, and intrinsic immunity. *Retrovirology* **5,** 51 (2008).
7. Yu, X. *et al.* Induction of APOBEC3G ubiquitination and degradation by an HIV-1 Vif-CUL5-SCF complex. *Science* **302,** 1056–1060 (2003).

8. Mehle, A., Goncalves, J., Santa-Marta, M., McPike, M. & Gabuzda, D. Phosphorylation of a novel SOCS-box regulates assembly of the HIV-1 Vif-CUL5 complex that promotes APOBEC3G degradation. *Genes Dev.* **18,** 2861–2866 (2004).
9. Yu, Y., Xiao, Z., Ehrlich, E. S., Yu, X. & Yu, X. F. Selective assembly of HIV-1 Vif-CUL5-ElonginB-ElonginC E3 ubiquitin ligase complex through a novel SOCS box and upstream cysteines. *Genes Dev.* **18,** 2867–2872 (2004).
10. Stopak, K., de Noronha, C., Yonemoto, W. & Greene, W. C. HIV-1 Vif blocks the antiviral activity of APOBEC3G by impairing both its translation and intracellular stability. *Mol. Cell* **12,** 591–601 (2003).
11. Marin, M., Rose, K. M., Kozak, S. L. & Kabat, D. HIV-1 Vif protein binds the editing enzyme APOBEC3G and induces its degradation. *Nature Med.* **9,** 1398–1403 (2003).
12. Conticello, S. G., Harris, R. S. & Neuberger, M. S. The Vif protein of HIV triggers degradation of the human antiretroviral DNA deaminase APOBEC3G. *Curr. Biol.* **13,** 2009–2013 (2003).
13. Sheehy, A. M., Gaddis, N. C. & Malim, M. H. The antiretroviral enzyme APOBEC3G is degraded by the proteasome in response to HIV-1 Vif. *Nature Med.* **9,** 1404–1407 (2003).
14. Mehle, A. *et al.* Vif overcomes the innate antiviral activity of APOBEC3G by promoting its degradation in the ubiquitin-proteasome pathway. *J. Biol. Chem.* **279,** 7792–7798 (2003).
15. de Bruijn, M. F. & Speck, N. A. Core-binding factors in hematopoiesis and immune function. *Oncogene* **23,** 4238–4248 (2004).
16. Ito, Y. RUNX genes in development and cancer: regulation of viral gene expression and the discovery of RUNX family genes. *Adv. Cancer Res.* **99,** 33–76 (2008).
17. Tahirov, T. H. *et al.* Structural analyses of DNA recognition by the AML1/Runx-1 Runt domain and its allosteric control by CBFβ. *Cell* **104,** 755–767 (2001).
18. Bravo, J., Li, Z., Speck, N. A. & Warren, A. J. The leukemia-associated AML1 (Runx1)–CBFβ complex functions as a DNA-induced molecular clamp. *Nature Struct. Biol.* **8,** 371–378 (2001).
19. Yan, J., Liu, Y., Lukasik, S. M., Speck, N. A. & Bushweller, J. H. CBFβ allosterically regulates the Runx1 Runt domain via a dynamic conformational equilibrium. *Nature Struct. Mol. Biol.* **11,** 901–906 (2004).
20. Liu, B., Sarkis, P. T., Luo, K., Yu, Y. & Yu, X. F. Regulation of Apobec3F and human immunodeficiency virus type 1 Vif by Vif-CUL5-ElonB/C E3 ubiquitin ligase. *J. Virol.* **79,** 9579–9587 (2005).
21. Simon, V. *et al.* Natural variation in Vif: differential impact on APOBEC3G/3F and a potential role in HIV-1 diversification. *PLoS Pathog.* **1,** e6 (2005).
22. Tian, C. *et al.* Differential requirement for conserved tryptophans in human immunodeficiency virus type 1 Vif for the selective suppression of APOBEC3G and APOBEC3F. *J. Virol.* **80,** 3112–3115 (2006).
23. Schröfelbauer, B., Senger, T., Manning, G. & Landau, N. R. Mutational alteration of human immunodeficiency virus type 1 Vif allows for functional interaction with nonhuman primate APOBEC3G. *J. Virol.* **80,** 5984–5991 (2006).
24. Russell, R. A. & Pathak, V. K. Identification of two distinct human immunodeficiency virus type 1 Vif determinants critical for interactions with human APOBEC3G and APOBEC3F. *J. Virol.* **81,** 8201–8210 (2007).
25. Mehle, A. *et al.* Identification of an APOBEC3G binding site in human immunodeficiency virus type 1 Vif and inhibitors of Vif-APOBEC3G binding. *J. Virol.* **81,** 13235–13241 (2007).
26. He, Z., Zhang, W., Chen, G., Xu, R. & Yu, X. F. Characterization of conserved motifs in HIV-1 Vif required for APOBEC3G and APOBEC3F interaction. *J. Mol. Biol.* **381,** 1000–1011 (2008).
27. Zhang, W., Chen, G., Niewiadomska, A. M., Xu, R. & Yu, X. F. Distinct determinants in HIV-1 Vif and human APOBEC3 proteins are required for the suppression of diverse host anti-viral proteins. *PLoS ONE* **3,** e3963 (2008).
28. Cao, W., Adya, N., Britos-Bray, M., Liu, P. P. & Friedman, A. D. The core binding factor (CBF) α interaction domain and the smooth muscle myosin heavy chain (SMMHC) segment of CBFβ-SMMHC are both required to slow cell proliferation. *J. Biol. Chem.* **273,** 31534–31540 (1998).

Supplementary Information is linked to the online version of the paper at www.nature.com/nature.

Acknowledgements We thank K. Strebel, A. Friedman, N. Speck, D. Yue, R. Siliciano, M. Malim, R. Harris, T. Inoue and D. Gabuzda for critical reagents; T. Wang, K. Zhao, X. Zhou and A. Zhen for technical assistance; R. Markham, J. Margolick and J. Bream for thoughtful discussions; and D. McClellan for editorial assistance. We also wish to thank staff within the Mass Spectrometry Core and the Institute for Basic Biomedical Sciences Microscope Facility at Johns Hopkins School of Medicine for their technical assistance. The following reagents were obtained through the AIDS Research and Reference Reagents Program, Division of AIDS, NIAID, NIH: monoclonal antibodies against HIV-1 p24 (B. Chesebro and H. Chen), pNL4-3 (M. Martin), pcDNA-hVif (S. Bour and K. Strebel), antiserum to HIV-1 Vif (D. Gabuzda) and MAGI-CCR5 cells (J. Overbaugh). This work was supported in part by funding from the Chinese Ministry of Science and Technology (2012CB911100) and Chinese Ministry of Education (IRT1016), the Key Laboratory of Molecular Virology, Jilin Province (20102209), China, and a grant (2R56AI62644-6) from the NIAID.

Author Contributions W.Z., J.D., S.L.E. and Y.Y. performed experiments and analysed the data. X.-F.Y. directed the project, analysed the data, and wrote the paper with help from all authors.

Author Information Reprints and permissions information is available at www.nature.com/reprints. The authors declare no competing financial interests. Readers are welcome to comment on the online version of this article at www.nature.com/nature. Correspondence and requests for materials should be addressed to X-F.Y. (xfyu@jhsph.edu).

METHODS

Plasmid construction. CBF-β coding sequences were amplified by reverse transcription and PCR using mRNA samples from H9 cells with the following primers: forward 5′-GCTAGCAAGATGCCGCGCGTCGTG-3′, reverse 5′-AAGCTTACTACAGATCTTCTTCTGATATGAGTTTTTGTTCGGGTCTTGTTGTCTTCTTGCC-3′, containing NheI and HindIII sites. The PCR product was cloned into pcDNA3.1 to generate pCBF-β-Myc. pCBF-βΔN1, CBF-βΔN2, CBF-βΔN3, CBF-βΔN4, CBF-βΔN5 and CBF-βΔN6 were made from pCBF-β-Myc by site-directed mutagenesis and confirmed by DNA sequencing. The following expression vectors have been previously described[7,20,29,30]: VR1012, HIV-1 Vif expression vectors pVif-Myc and pVif-HA, pAPOBEC3G-HA, pAPOBEC3G-Myc, pUbiquitin-Myc, pCUL5-HA, pAPOBEC3F-V5, E4orf6-Myc, SOCS3-HA, human p53, SIV_{MAC}Vif-HA, SIV_{AGM}Vif-Myc, BIVVif-HA, HXB2Neo and HXB2NeoVif-HA. pVifΔN-HA was constructed with the following primers: forward 5′-GTCGACATGGACCCTGAACTAGC-3′, reverse 5′-GGAATTCCTACGCGTAATCTGGGACGTCGTAAGGGTAGTGTTCCATTCATTGTGTGGCT-3′, containing SalI and NotI sites, respectively, and a C-terminal HA tag. pNL4-3ΔVif and pcDNA-hVif were gifts from K. Strebel. pRUNX1-Myc and $p(CBF)_4$TKLuc were gifts from A. Friedman. NL43-ΔE-EGFP was a gift from R. Silicano. Plasmids pVifW11A, W21A, W38A, DR14/15AA, K22E, Y40A, RH41/42AA, T74A, E76A, R77A and W79A were made from pVif-Myc by site-directed mutagenesis and confirmed by DNA sequencing. To generate YFP N-terminal epitope-tagged NL4-3 Vif, pcDNA-hVif was used to PCR amplify the Vif coding region and cloned into the NotI and XbaI sites of pcDNA3-YFP (D. T. Yue). To generate CFP N-terminal epitope-tagged CBF-β, the CBF-β coding region was cloned into the NotI and XbaI sites of pcDNA3-CFP (D. T. Yue). The YFP–CFP dimer construct was gift from D. T. Yue and was generated by fusing CFP and YFP with a 21 amino acid linker, SRAQASNSAVDGTAGPGSIAT. The following CBF-β shRNA clones were obtained from Open Biosystems: TRCN0000016643, with mature sense sequence 5′-CGAGAGTATGTCGACTTAGAA-3′; TRCN0000016644, 5′-CCGCGAGTGTGAGATTAAGTA-3′; TRCN0000016645, 5′-GAAGATAGAGACAGGTCTCAT-3′; TRCN0000016646, 5′-GCTGGCAGTAACTGGCAAGAA-3′; TRCN0000016647, 5′-TGAGATTAAGTACACGGGCT-3′.

Antibodies and cell lines. The H9 human $CD4^+$ T-cell line was maintained in RPMI-1640 medium (Invitrogen) with 10% fetal bovine serum and penicillin/streptomycin (R-10 medium). 293T and MAGI-CCR5 cells (AIDS Research and Reference Reagents Program, catalogue no. 3522) were maintained in Dulbecco's modified Eagle's medium (DMEM; Invitrogen) with 10% fetal bovine serum and penicillin/streptomycin (D-10 medium) and passaged when confluent. The following antibodies were used: anti-HA (Covance, MMS-101R-1000), anti-Myc (Upstate, 05-724), anti-V5 (Invitrogen, R960-25), anti-β-actin (Sigma, A3853), anti-histone H3 (Genscript, A01502), anti-human ribosomal P antigens (Immunovision, HP0-0100), anti-HA antibody–agarose conjugate (Roche, 11815016001), anti-ELOB (Santa Cruz, sc-1558), anti-ELOC (BD Transduction Lab, SIII/P15, 610760), anti-GAPDH (Sigma, G8795), anti-CBF-β (Abcam, ab11921), anti-CUL5 (Santa Cruz, sc-13014), anti-p53 (Oncogene Research Products, OP03) and anti-GFP (Genscript, A01704); anti-CAp24 (catalogue no. 1513) and anti-Vif antibodies (catalogue no. 2221) were obtained from the AIDS Research and Reference Reagents Program.

RNA interference. RNAi against CBF-β was carried out using a pool of two duplexed siRNAs (Dharmacon): duplex 1, sense, 5′-CCAGCAGGAGGAUGCAUUAUU; antisense, 5′-PUAAUGCAUCCUCCUGCUGGUU; duplex 2, sense, 5′-GCAGGCAAGGUAUAUUUGAUU; antisense, 5′-PUCAAAUAUACCUUGCCUGCUU. RNAi against CUL5 was carried out using a pool of four duplexed siRNAs (Dharmacon): duplex 1, sense, 5′-GACACGACGUCUUAUAUUAUU; antisense, 5′-PUAAUAUAAGACGUCGUGUCUU; duplex 2, sense, 5′-CGUCUAAUCUGUUAAAGAAUU; antisense, 5′-PUUCUUUAACAGAUUAGACGUU; duplex 3, sense, 5′-GAUGAUACGGCUUUGCUAAUU; antisense, 5′-PUUAGCAAAGCCGUAUCAUCUU; duplex 4, sense, 5′-GUUCAACUACGAAUACUAAUU; antisense, 5′-PUUAGUAUUCGUAGUUGAACUU. 293T cells were transfected with the CBF-β or CUL5 siRNA pool at a total final concentration of 100 nM using Lipofectamine 2000 (Invitrogen). The non-targeting siRNA no. 2 (Dharmacon) was used as a control. Protein expression was monitored by immunoblotting 2–3 days after transfection.

Identification of Vif-binding proteins. Vif-containing complexes were purified from HIV-1 Vif–HA and control HIV-1 (HXB2Neo) infected H9 cells by immunoprecipitation and analysed by SDS–PAGE. Gels were fixed in 50% methanol/10% acetic acid for 10 min, stained with mass spectrometry-compatible colloidal-Coomassie brilliant blue G-250 (Bio-Rad 1610406) staining solution (20% methanol, 8% ammonium sulphate, 1.6% phosphoric acid, 0.08% Coomassie blue G-250) to detect protein bands, and de-stained with distilled water. Protein standards from Bio-Rad (catalogue no. 1610314) were used to estimate protein size. Protein bands of interest were cut out of the gel and rinsed twice with 50% methanol (HPLC grade). In-gel digestion was performed on protein bands cut out of colloidal-Coomassie blue-stained SDS–polyacrylamide gels using sequencing-grade modified trypsin (Promega). Extracted peptides were co-crystallized in 2,5-dihydroxybenozic acid (DHB) or α-cyano-4-hydroxycinnamic acid (CHCA) (10 mg ml^{-1} in 50% acetonitrile/0.3% TFA) and analysed by matrix-assisted laser desorption ionization time-of-flight (MALDI-TOF) spectrometry on a Voyager DE STR (Applied Biosystems, http://www.appliedbiosystems.com) using Voyager Instrument Control Panel (v. 5.1) and Data Explorer (v. 4.0) software. Data were acquired in reflector mode, and masses were externally calibrated using a standard peptide mixture to $<$50 p.p.m. error. Proteins were identified by searching the acquired monoisotopic masses against the NCBI non-redundant or SwissProt databases using the MS-Fit search engine of ProteinProspector (http://prospector.ucsf.edu).

APOBEC3G ubiquitination assay. 293T cells were transfected with expression vectors encoding APOBEC3G–HA, HIV-1 Vif and ubiquitin–Myc, either individually or in combination. Cells were also transfected with control or CBF-β-specific siRNA. Transfected cells were treated with 10 μM MG132 (proteasome inhibitor) for 16 h, beginning at 24 h after transfection, and then lysed in lysis buffer (50 mM Tris, pH 7.5, with 150 mM NaCl, 1% Triton X-100, 1 mM EDTA, 10 μM MG132 and complete protease inhibitor cocktail tablets), followed by centrifugation at 10,000*g* for 30 min. Lysates were applied to anti-HA antibody-conjugated agarose beads (Roche) and incubated for 3 h at 4 °C. After incubation, the beads were washed six times with washing buffer (20 mM Tris, pH 7.5, with 0.1 M NaCl, 0.1 mM EDTA and 0.05% Tween 20), then eluted with elution buffer (0.1 M glycine-HCl, pH 2.0) followed by SDS–PAGE and immunoblotting with anti-Myc and anti-HA antibodies.

Transfection, virus purification, immunoblot analysis, immunoprecipitation and viral infectivity (MAGI) assays were performed as previously described[7,29].

29. Luo, K. *et al.* Primate lentiviral virion infectivity factors are substrate receptors that assemble with cullin 5–E3 ligase through a HCCH motif to suppress APOBEC3G. *Proc. Natl Acad. Sci. USA* **102,** 11444–11449 (2005).
30. Luo, K. *et al.* Adenovirus E4orf6 assembles with Cullin5-ElonginB-ElonginC E3 ubiquitin ligase through an HIV/SIV Vif-like BC-box to regulate p53. *FASEB J.* **21,** 1742–1750 (2007).

LETTER

doi:10.1038/nature10693

Vif hijacks CBF–β to degrade APOBEC3G and promote HIV–1 infection

Stefanie Jäger[1,2]*, Dong Young Kim[3]*, Judd F. Hultquist[4]*, Keisuke Shindo[4], Rebecca S. LaRue[4], Eunju Kwon[3], Ming Li[4], Brett D. Anderson[4], Linda Yen[3], David Stanley[3], Cathal Mahon[1,2,3], Joshua Kane[1,2], Kathy Franks-Skiba[1,2], Peter Cimermancic[2,5], Alma Burlingame[2,3], Andrej Sali[2,3,5,6], Charles S. Craik[2,3], Reuben S. Harris[4], John D. Gross[2,3,6] & Nevan J. Krogan[1,2,6,7]

Restriction factors, such as the retroviral complementary DNA deaminase APOBEC3G, are cellular proteins that dominantly block virus replication[1–3]. The AIDS virus, human immunodeficiency virus type 1 (HIV-1), produces the accessory factor Vif, which counteracts the host's antiviral defence by hijacking a ubiquitin ligase complex, containing CUL5, ELOC, ELOB and a RING-box protein, and targeting APOBEC3G for degradation[4–10]. Here we reveal, using an affinity tag/purification mass spectrometry approach, that Vif additionally recruits the transcription cofactor CBF-β to this ubiquitin ligase complex. CBF-β, which normally functions in concert with RUNX DNA binding proteins, allows the reconstitution of a recombinant six-protein assembly that elicits specific polyubiquitination activity with APOBEC3G, but not the related deaminase APOBEC3A. Using RNA knockdown and genetic complementation studies, we also demonstrate that CBF-β is required for Vif-mediated degradation of APOBEC3G and therefore for preserving HIV-1 infectivity. Finally, simian immunodeficiency virus (SIV) Vif also binds to and requires CBF-β to degrade rhesus macaque APOBEC3G, indicating functional conservation. Methods of disrupting the CBF-β–Vif interaction might enable HIV-1 restriction and provide a supplement to current antiviral therapies that primarily target viral proteins.

Mammals have evolved cellular proteins termed restriction factors that function to prevent the spread of mobile genetic elements including retroviruses[1–3]. As a counter-defence, most retroviruses, including the human pathogen HIV-1, have developed mechanisms to prevent restriction, often through subversion of the host's ubiquitin–proteasome system. In eukaryotic cells, 8.6-kDa ubiquitin moieties are added to a target protein by sequential action of one of two ubiquitin-activating enzymes (E1), which transfer ubiquitin to a pool of dozens of ubiquitin-conjugating enzymes (E2) that, in turn, collaborate with hundreds of ubiquitin ligases (E3) to catalyse transfer to specific substrates[11]. If more than four ubiquitins are joined together through K48 linkages, the target protein is usually degraded by the 26S proteasome[12]. At least three HIV-1 proteins, Vif, Vpu and Vpr, hijack cullin-RING E3 ligases consisting of CUL5, CUL1 and CUL4A to promote ubiquitination and degradation of APOBEC3 family members (for example, APOBEC3G, A3G), BST2/tetherin and an unknown, putative restriction factor, respectively[2]. Understanding the composition of cullin-RING E3 ligase complexes and the underlying cellular signalling components may provide therapeutic routes for treating a variety of human diseases, including infection by HIV-1.

HIV-1 Vif is recruited to CUL5 by virtue of its SOCS box, which contains an elongin C binding helix (the BC-box), a conserved HCCH Zn binding motif and a short Cullin Box[4–6]. Although a structure of the BC-box peptide in complex with the heterodimer of Elongin B and C (ELOBC) has been reported[13], the architecture of the full-length Vif in complex with host factors has remained elusive, in part because Vif complexes have poor solubility and activity. We therefore reasoned that Vif may bind an additional host factor and that such a factor may render it more tractable *in vitro*.

We took an unbiased proteomic approach to identify host factors that bind all 18 HIV processed and polyproteins using an affinity tag/purification mass spectrometry (AP–MS) approach[14,15]. To this end, 2×Strep and 3×Flag was fused to the carboxy (C) terminus of these factors, including Vif. The tagged Vif construct was both transiently transfected into HEK293 cells and used to make a stable, tetracycline-inducible Vif–Strep–Flag Jurkat T cell line (Fig. 1a). Epitope-tagged Vif was purified from both cell types using antibodies specific to either Strep or Flag and aliquots of the co-purifying proteins were subjected to SDS–polyacrylamide gel electrophoresis (SDS–PAGE) (Fig. 1b). Materials from each step were analysed by mass spectrometry[14].

Using a new scoring system for data derived from AP–MS studies, termed Mass Spectrometry Interaction Statistics (MiST)[15], we identified 24 Vif–human protein–protein interactions with seven of them found in both cell types (Fig. 1c). Seventeen of these were verified independently by co-immunoprecipitation (Supplementary Fig. 1). Among these were the components of the E3 ubiquitin ligase complex, CUL5, ELOB and ELOC, known to interact with Vif and trigger A3G degradation[4–6,8–10]. Although the RING-box protein RBX1 was originally reported as part of this complex[4], only RBX2 was above the MiST score threshold used[15] consistent with recent work showing that it binds CUL5 (refs 16, 17). We did not find endogenous A3G, probably because of its poor expression in HEK293 and Jurkat cell lines exacerbated by further depletion through Vif-mediated degradation. We did find Vif associating with two proteins that function in autophagy, AMRA1 and SQSTM, as well as with the transcriptional co-repressor complex NCOR1/HDAC3/GPS2/TBL1R (the last only in T cells) (Fig. 1c). Also, in both cell types, Vif was found to interact with the transcription cofactor CBF-β, which is known to heterodimerize with the RUNX family of transcription factors[18].

To determine if any of the newly defined Vif interactors belong to the Vif–CUL5 complex, we performed double affinity purifications using cells co-transfected with Vif–2×Strep and either A3G– or CUL5–3×Flag (Fig. 1d, e). After purification first with Strep-Tactin and second with anti-Flag beads, mass spectrometry analysis of the final elution revealed the presence of CUL5, ELOB, ELOC, RBX2 and invariably CBF-β, strongly suggesting that this last protein may be a new component of the Vif E3 ubiquitin ligase complex (other factors from single Vif purifications depicted in Fig. 1c were not present). To confirm this interaction and the composition of the complex, we performed an additional double affinity purification experiment using

[1]Department of Cellular and Molecular Pharmacology, University of California-San Francisco, San Francisco, California 94158, USA. [2]California Institute for Quantitative Biosciences, QB3, San Francisco, California, California 94158, USA. [3]Department of Pharmaceutical Chemistry, University of California, San Francisco, California 94158, USA. [4]Department of Biochemistry, Molecular Biology and Biophysics, Institute for Molecular Virology, Center for Genome Engineering, University of Minnesota, Minneapolis, Minnesota 55455, USA. [5]Department of Bioengineering and Therapeutic Sciences, University of California, San Francisco, California 94158, USA. [6]HPC (Host Pathogen Circuitry) Group, University of California-San Francisco, San Francisco, California 94158, USA. [7]J. David Gladstone Institutes, San Francisco, California 94158, USA.
*These authors contributed equally to this work.

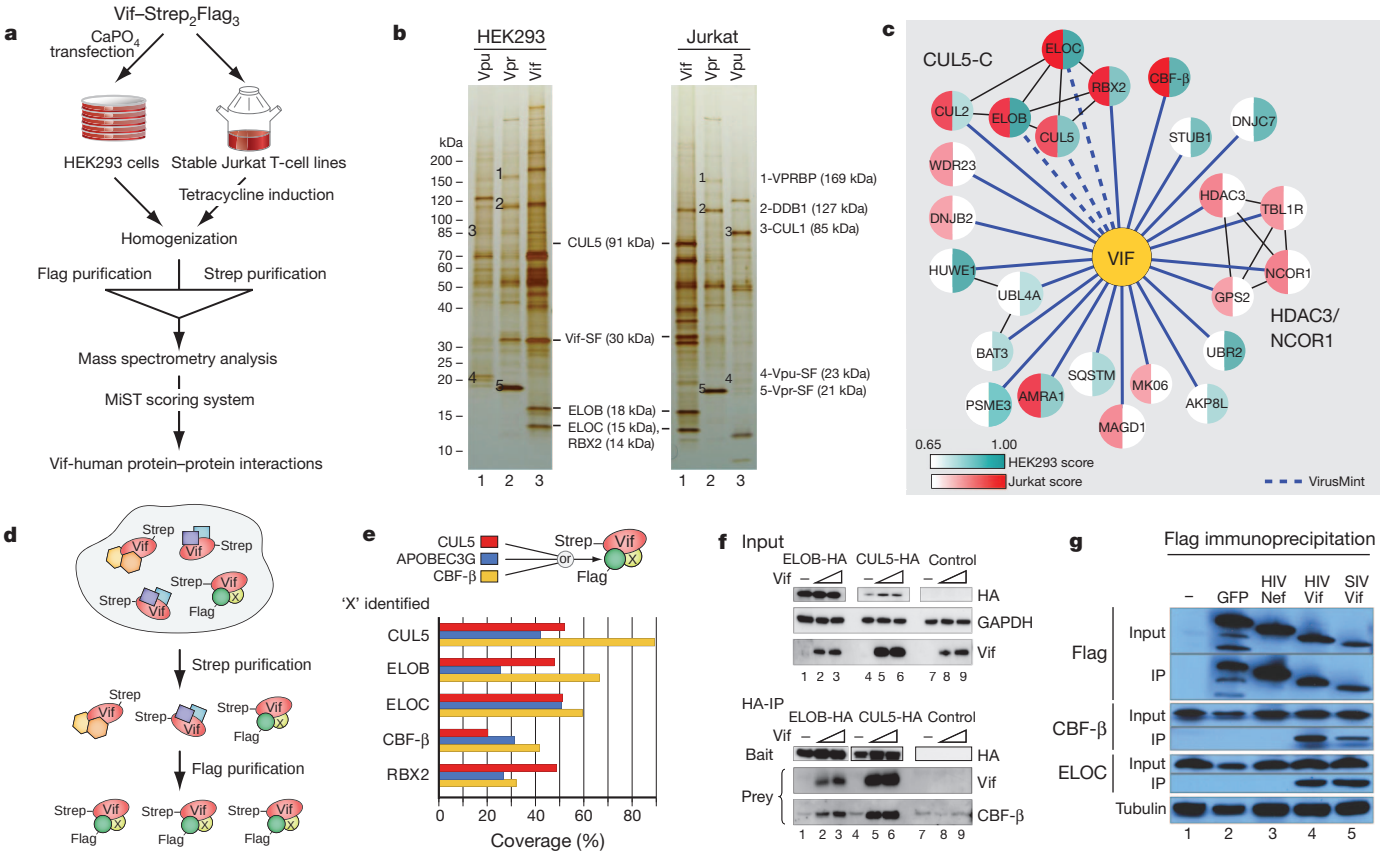

Figure 1 | AP–MS experiments identify CBF-β as a Vif-dependent component of the Vif–CUL5 ubiquitin ligase complex. a, Flow-chart of the proteomic analysis performed during the study. **b**, Affinity-tagged versions of Vif, Vpu and Vpr were purified using 3×Flag from HEK293 and Jurkat cells, subjected to SDS–PAGE and stained with silver. Visible bands corresponding to interactions that are known for each accessory factor are labelled. Note Vif and CBF-β run at a similar place on the gel. Tagged versions of Vpr and Vpu were used as specificity controls. **c**, A network representation of Vif–host protein–protein interactions from both HEK293 (blue) and Jurkat T cells (red) after subjecting the data derived from the AP–MS analysis to the MiST scoring system[15]. The intensity of the node colours corresponds to the quantitative MiST score. Blue edges represent interactions derived during this work; black edges are previously described interactions between host factors; dashed edges correspond to previously described Vif–host interactions present in the database VirusMint. **d**, The double purification approach, which allows for the identification of stable, stoichiometric protein complexes. **e**, Double purifications were performed in triplicate using 3×Flag-tagged CUL5, A3G or CBF-β with 2×Strep-tagged Vif in HEK293 cells. Proteins that were identified in all three double purifications, after trypsin digestion and analysis by mass spectrometry, are represented. The coverage corresponds to the percentage of protein identified by tryptic peptides. **f**, Immunoblots showing that Vif recruits CBF-β to the CUL5/ELOBC/RBX2 ubiquitin ligase complex. HA-tagged ELOB or CUL5 were immunoprecipitated in the absence or presence of increasing amounts of Vif, and endogenous CBF-β was monitored by immunoblot. **g**, HIV and SIV Vif co-immunoprecipitate CBF-β and ELOC. GFP and HIV Nef were analysed in parallel as specificity controls.

Vif–2×Strep and CBF-β–3×Flag. This strategy also yielded CUL5, ELOB, ELOC and RBX2, in addition to the epitope-tagged bait proteins (Fig. 1d, e).

To determine if the association of CBF-β with the CUL5 ligase complex was dependent on Vif, we immunoprecipitated CUL5-haemagglutinin (HA) or ELOB-HA in the presence or absence of Vif in HEK293 cells and blotted for endogenous CBF-β. Only in the presence of Vif did CBF-β co-immunoprecipitate with tagged CUL5 or ELOB, indicating that recruitment of CBF-β to the CUL5 ligase is dependent on Vif (Fig. 1f). SIV Vif also associated with CBF-β by immunoprecipitation, suggesting the interaction is conserved (Fig. 1g).

We next asked if the Vif–CUL5 ligase could be reconstituted with CBF-β using recombinant proteins purified from *Escherichia coli*. Initial purification attempts without CBF-β yielded aggregated and inactive complexes, assayed by size-exclusion chromatography and autoubiquitination activity, suggesting that CBF-β may be required for complex formation (data not shown). Therefore, full-length Vif, ELOB, ELOC and CBF-β were co-expressed, purified to homogeneity and found to form a stable, monodisperse complex with recombinant CUL5/RBX2, as shown by size-exclusion chromatography and SDS–PAGE analysis (Fig. 2a, b). Pull-down experiments performed with purified, His-tagged APOBEC3 enzymes immobilized on cobalt-chelating resin showed that the four protein complex containing Vif, CBF-β and ELOBC binds A3G, but not the related Vif-resistant deaminase, A3A (Fig. 2c). These observations suggested that Vif, CBF-β and ELOBC form a substrate adaptor for CUL5/RBX2 that enables specific interaction with susceptible A3 proteins.

To test the activity of the reconstituted six protein complex, CUL5/RBX2/ELOB/ELOC/Vif/CBF-β (CRL5–Vif–CBF-β), we assayed substrate and Vif ubiquitination activities using two distinct and well characterized ubiquitin conjugating enzymes, UBE2R1 (hCDC34a) and UBCH5b, which are capable of forming specific K48 and heterogenous ubiquitin chain linkages, respectively[19,20]. With UBE2R1, CRL5–Vif–CBF-β catalysed formation of high-molecular mass K48 chains on A3G, but not A3A (Fig. 2d, e), mirroring the chain linkage and substrate specificity observed in cells[4,6,21–23]. As with most ubiquitin ligase assemblies, the CRL5–Vif–CBF-β complex also possessed autoubiquitination activity that was only marginally affected by substrate A3s (Supplementary Fig. 2). These experiments were done with NEDD8-modified CUL5, because NEDD8ylation is required for CUL5 to degrade A3G *in vivo*[4] (Supplementary Fig. 3). Similarly, with UBCH5b, CRL5–Vif–CBF-β was able to promote the specific polyubiquitination of A3G and elicit Vif autoubiquitination activity (Supplementary Fig. 4). We conclude that the reconstituted Vif E3 ligase is specific for A3G,

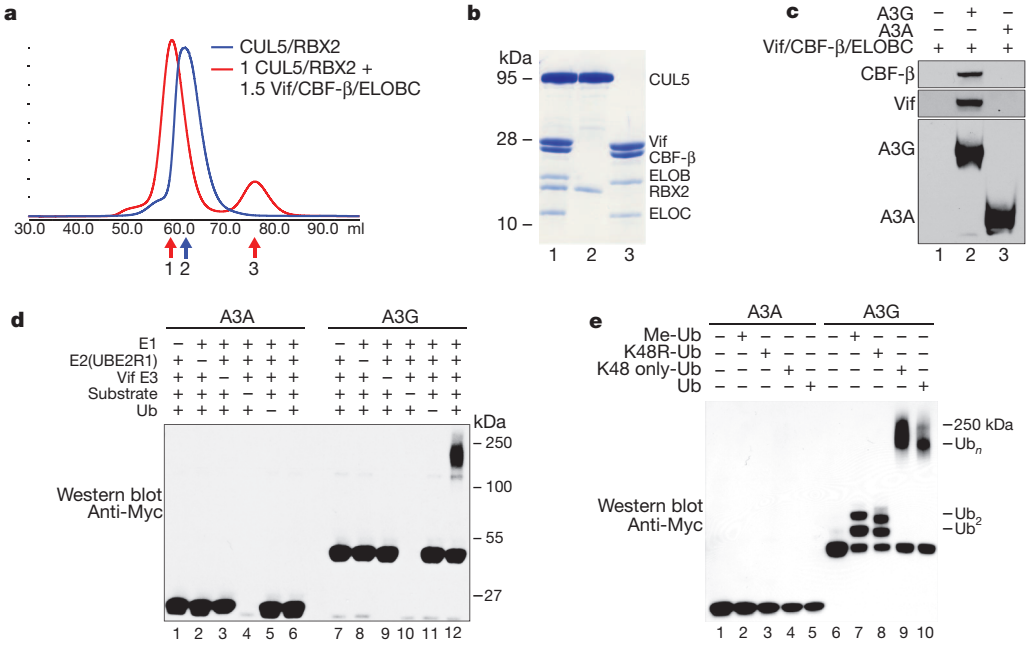

Figure 2 | CBF-β is a stoichiometric component of the Vif E3 ubiquitin ligase. **a**, Size exclusion chromatography of recombinant purified CUL5/RBX2 (blue) overlaid with CUL5/RBX2 mixed with 1.5 equivalents of purified Vif substrate adaptor containing Vif, ELOBC and CBF-β (red). **b**, Coomassie-stained SDS–PAGE of fractions labelled 1–3 in **a** indicating the Vif substrate adaptor and a six-protein assembly (CRL5–Vif–CBF-β) co-purify as stable monodisperse species. **c**, A3G, but not A3A, directly binds the tetrameric Vif substrate adaptor in pull-down experiments *in vitro*. **d**, CRL5–Vif–CBF-β is an E3 ligase that promotes polyubiquitination of A3G, but not A3A (detected using an anti-c-Myc antibody to the C-terminal tag on the deaminases). Ub, ubiquitin. **e**, CRL5–Vif–CBF-β and UBE2R1 catalyse formation of K48-linked chains on A3G. Immunoblots showing substrate in ubiquitination reactions containing UBE2R1 as E2, no ubiquitin, Me-ubiquitin, K48R-ubiquitin, K48-only ubiquitin or wild-type ubiquitin. Reactions with Me-ubiquitin indicate at least two distinct sites are modified on A3G; K48R recapitulates the pattern observed with Me-ubiquitin, whereas both wild type and K48R-only ubiquitin result in extensive polyubiquitin chains.

supports K48 chain formation and can function with at least two ubiquitin conjugating enzymes *in vitro*. It is conceivable that these two ubiquitin-conjugating enzymes work together in cells to promote multi-monoubiquitination of A3G followed by specific chain elongation, as described for other RING E3s[24,25], but additional work will be necessary to rule out other E2s *in vivo*.

To determine if CBF-β is required for Vif folding and/or stability in living cells, we transfected a constant amount of Vif into HEK293T cells expressing either a scrambled short hairpin (sh)RNA or a CBF-β-specific shRNA. The levels of steady-state Vif were threefold lower in CBF-β-depleted cells than in the scrambled control cells (Fig. 3a). Proteasome inhibitor MG132 reversed this effect, suggesting that Vif

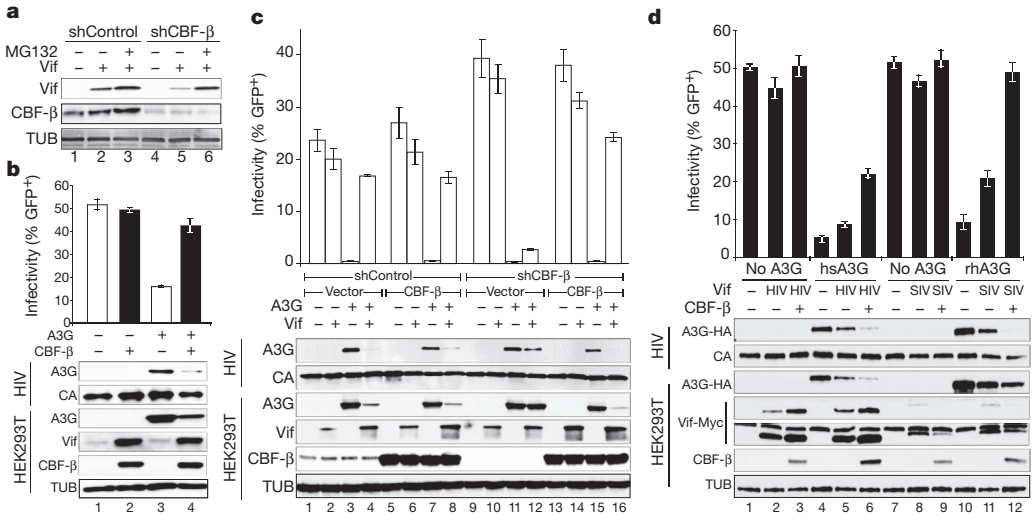

Figure 3 | CBF-β and Vif collaborate to degrade APOBEC3G and enable HIV-1 infectivity. **a**, CBF-β-depleted HEK293T cells have lower steady-state Vif levels, which recover upon treatment with 2.5 μM MG132. **b**, Infectivity of replication-competent, Vif-proficient HIV-1 in the presence and absence of CBF-β and A3G ($n = 3$; mean, s.d.). Immunoblots are shown for the indicated proteins in virus-producing cells and viral particles. **c**, Infectivity of HIV-GFP produced using HEK293T-shCBF-β or HEK293T-shControl clones transfected with the single-cycle virus cocktail, A3G, Vif and CBF-β as indicated ($n = 3$; mean, s.d.). The corresponding immunoblots are shown below. **d**, Infectivity of a Vif-deficient HIV-1 molecular clone produced in the presence or absence of human or rhesus A3G-HA, HIV or SIV Vif–Myc, and CBF-β as indicated ($n = 3$; mean, s.d.). Immunoblots are shown for the indicated proteins in virus-producing cells and viral particles with two exposures of the anti-Myc (Vif) blot shown to clarify the SIV Vif signal (the longer exposure also shows endogenous c-Myc).

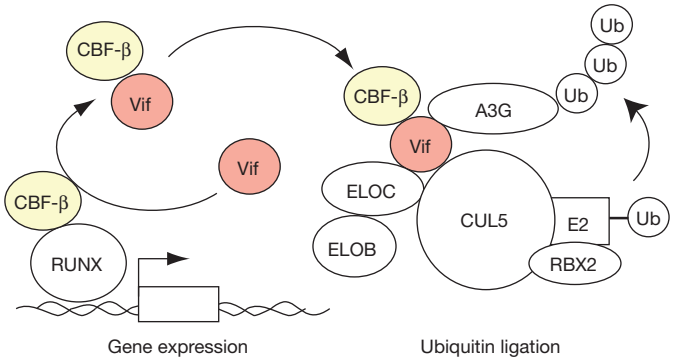

Figure 4 | Model for Vif–CBF-β E3 ligase formation and APOBEC3G polyubiquitination and degradation. Vif is depicted hijacking cellular CBF-β to the E3 ubiquitin ligase complex required for A3G polyubiquitination and degradation. Vif may recruit newly translated CBF-β (not shown) and/or hijack existing CBF-β from RUNX transcription complexes.

degradation is accelerated without CBF-β. Analogous data were obtained when Vif was expressed from a proviral plasmid in CBF-β-depleted cells and complemented with a CBF-β expression plasmid (Supplementary Fig. 5).

Based on these observations, we predicted that CBF-β knockdown should result in less functional Vif and less infectious HIV-1 particles when produced in the presence of A3G. To test this prediction, shRNA was used to deplete CBF-β stably in HEK293T cells, and a knockdown clone was used to produce replication competent Vif-proficient HIV-1 in the presence or absence of A3G and CBF-β expressed from plasmids (Fig. 3b). In CBF-β depleted cells, steady-state Vif levels were very low despite equivalent levels of virus production as indicated by capsid. Moreover, Vif levels increased when CBF-β was replenished by complementation, and this correlated with decreases in cellular and viral A3G levels and corresponding increases in viral infectivity. In the absence of A3G, no difference in infectivity was observed regardless of cellular CBF-β or Vif levels. Titration experiments showed that CBF-β complementation is dose-responsive (Supplementary Fig. 6). Analogous results were obtained with a multi-vector HIV/green fluorescent protein (GFP) system (Fig. 3c and Supplementary Fig. 7). The Vif/CBF-β interaction was confirmed in virus-producing cells by co-immunoprecipitation experiments (Supplementary Fig. 8). Furthermore, SIVmac239 Vif requires CBF-β to degrade rhesus macaque A3G and promote viral infectivity (Fig. 3d). Interestingly, in contrast to HIV Vif, lower steady-state levels of SIV Vif were observed in the presence of CBF-β, which may be functionally significant or may be a consequence of the heterologous assay system (that is, expressing SIV/rhesus proteins in human cells). Nevertheless, these results demonstrate the essential and conserved nature of CBF-β for Vif function in promoting A3G degradation and efficient virus replication.

Our proteomic, biochemical and genetic studies combine to suggest a model in which HIV-1 Vif hijacks the cellular transcription factor CBF-β to facilitate Vif folding and/or stability as well as nucleation of the rest of the E3 ubiquitin ligase complex (Fig. 4). CBF-β is required for A3G substrate binding and, ultimately, for polyubiquitination and degradation, thereby enabling the production of infectious viral particles. Because genetic studies have shown that Vif is also capable of degrading APOBEC3F and several other human APOBEC3 proteins[2,3,23] most of which are expressed in primary CD4+ T lymphocytes[26,27], it is quite likely that CBF-β is required for counteracting multiple endogenous APOBEC3s and thus for rendering T lymphocytes permissive for HIV-1 replication. We anticipate that the development of antiviral therapies that antagonize the CBF-β–Vif interaction will be more powerful than those that specifically target the A3G–Vif interaction, because they have the potential to unleash the simultaneous restriction potential of multiple APOBEC3s analogous to current combinatorial therapies.

METHODS SUMMARY

Affinity tagging, purification[14] and ubiquitination assays[28] were performed as described. Recombinant A3A and A3G were purified as Myc-His tagged proteins from HEK293 cells. HIV-1 infectivity studies used an HIV-1_{IIIB} proviral DNA construct (with or without Vif) or an HIV-GFP reporter plasmid set. Control (RHS4346) and CBF-β (RHS4430-99161432) shRNA constructs were obtained from Open Biosystems. A CBF-β complementary DNA matching NM_001755.2 was cloned from the CEM T cell line by RT–PCR. Immunoblots used antibodies to A3G (National Institutes of Health (NIH) ARRRP 10201 courtesy of J. Lingappa), CBF-β (Santa Cruz Biotechnology), HA (HA.11; Covance), TUB (tubulin; Covance), c-Myc (Sigma), Vif (NIH ARRRP 2221 courtesy of D. Gabuzda) and p24/capsid (NIH ARRRP 3537 courtesy of B. Chesebro and K. Wehrly). Details are provided in the Supplementary Methods.

Received 26 March; accepted 1 November 2011.
Published online 21 December 2011.

1. Goff, S. P. Retrovirus restriction factors. *Mol. Cell* **16,** 849–859 (2004).
2. Malim, M. H. & Emerman, M. HIV-1 accessory proteins—ensuring viral survival in a hostile environment. *Cell Host Microbe* **3,** 388–398 (2008).
3. Albin, J. S. & Harris, R. S. Interactions of host APOBEC3 restriction factors with HIV-1 *in vivo*: implications for therapeutics. *Expert Rev. Mol. Med.* **12,** e4 (2010).
4. Yu, X. *et al.* Induction of APOBEC3G ubiquitination and degradation by an HIV-1 Vif-Cul5-SCF complex. *Science* **302,** 1056–1060 (2003).
5. Mehle, A., Goncalves, J., Santa-Marta, M., McPike, M. & Gabuzda, D. Phosphorylation of a novel SOCS-box regulates assembly of the HIV-1 Vif-Cul5 complex that promotes APOBEC3G degradation. *Genes Dev.* **18,** 2861–2866 (2004).
6. Mehle, A. *et al.* Vif overcomes the innate antiviral activity of APOBEC3G by promoting its degradation in the ubiquitin-proteasome pathway. *J. Biol. Chem.* **279,** 7792–7798 (2004).
7. Sheehy, A. M., Gaddis, N. C., Choi, J. D. & Malim, M. H. Isolation of a human gene that inhibits HIV-1 infection and is suppressed by the viral Vif protein. *Nature* **418,** 646–650 (2002).
8. Sheehy, A. M., Gaddis, N. C. & Malim, M. H. The antiretroviral enzyme APOBEC3G is degraded by the proteasome in response to HIV-1 Vif. *Nature Med.* **9,** 1404–1407 (2003).
9. Conticello, S. G., Harris, R. S. & Neuberger, M. S. The Vif protein of HIV triggers degradation of the human antiretroviral DNA deaminase APOBEC3G. *Curr. Biol.* **13,** 2009–2013 (2003).
10. Stopak, K., de Noronha, C., Yonemoto, W. & Greene, W. C. HIV-1 Vif blocks the antiviral activity of APOBEC3G by impairing both its translation and intracellular stability. *Mol. Cell* **12,** 591–601 (2003).
11. Passmore, L. A. & Barford, D. Getting into position: the catalytic mechanisms of protein ubiquitylation. *Biochem. J.* **379,** 513–525 (2004).
12. Thrower, J. S., Hoffman, L., Rechsteiner, M. & Pickart, C. M. Recognition of the polyubiquitin proteolytic signal. *EMBO J.* **19,** 94–102 (2000).
13. Stanley, B. J. *et al.* Structural insight into the human immunodeficiency virus Vif SOCS box and its role in human E3 ubiquitin ligase assembly. *J. Virol.* **82,** 8656–8663 (2008).
14. Jäger, S. *et al.* Purification and characterization of HIV-human protein complexes. *Methods* **53,** 13–19 (2011).
15. Jäger, S. *et al.* Global landscape of HIV–human protein complexes. *Nature* doi:10.1038/nature10719 (this issue).
16. Kamura, T. *et al.* VHL-box and SOCS-box domains determine binding specificity for Cul2-Rbx1 and Cul5-Rbx2 modules of ubiquitin ligases. *Genes Dev.* **18,** 3055–3065 (2004).
17. Huang, D. T. *et al.* E2-RING expansion of the NEDD8 cascade confers specificity to cullin modification. *Mol. Cell* **33,** 483–495 (2009).
18. Wong, W. F., Kohu, K., Chiba, T., Sato, T. & Satake, M. Interplay of transcription factors in T-cell differentiation and function: the role of Runx. *Immunology* **132,** 157–164 (2011).
19. Petroski, M. D. & Deshaies, R. J. Mechanism of lysine 48-linked ubiquitin-chain synthesis by the cullin-RING ubiquitin-ligase complex SCF-Cdc34. *Cell* **123,** 1107–1120 (2005).
20. Kim, H. T. *et al.* Certain pairs of ubiquitin-conjugating enzymes (E2s) and ubiquitin-protein ligases (E3s) synthesize nondegradable forked ubiquitin chains containing all possible isopeptide linkages. *J. Biol. Chem.* **282,** 17375–17386 (2007).
21. DeHart, J. L., Bosque, A., Harris, R. S. & Planelles, V. Human immunodeficiency virus type 1 Vif induces cell cycle delay via recruitment of the same E3 ubiquitin ligase complex that targets APOBEC3 proteins for degradation. *J. Virol.* **82,** 9265–9272 (2008).
22. Stenglein, M. D., Burns, M. B., Li, M., Lengyel, J. & Harris, R. S. APOBEC3 proteins mediate the clearance of foreign DNA from human cells. *Nature Struct. Mol. Biol.* **17,** 222–229 (2010).
23. Hultquist, J. F. *et al.* Human and rhesus APOBEC3D, APOBEC3F, APOBEC3G, and APOBEC3H demonstrate a conserved capacity to restrict Vif-deficient HIV-1. *J. Virol.* **85,** 11220–11234 (2011).
24. Rodrigo-Brenni, M. C. & Morgan, D. O. Sequential E2s drive polyubiquitin chain assembly on APC targets. *Cell* **130,** 127–139 (2007).
25. Wu, K., Kovacev, J. & Pan, Z. Q. Priming and extending: a UbcH5/Cdc34 E2 handoff mechanism for polyubiquitination on a SCF substrate. *Mol. Cell* **37,** 784–796 (2010).

26. Koning, F. A. *et al.* Defining APOBEC3 expression patterns in human tissues and hematopoietic cell subsets. *J. Virol.* **83,** 9474–9485 (2009).
27. Refsland, E. W. *et al.* Quantitative profiling of the full *APOBEC3* mRNA repertoire in lymphocytes and tissues: implications for HIV-1 restriction. *Nucleic Acids Res.* **38,** 4274–4284 (2010).
28. Saha, A. & Deshaies, R. J. Multimodal activation of the ubiquitin ligase SCF by Nedd8 conjugation. *Mol. Cell* **32,** 21–31 (2008).

Supplementary Information is linked to the online version of the paper at www.nature.com/nature.

Acknowledgements We thank members of the Krogan, Gross and Harris laboratories for comments, J. R. Johnson for mass spectrometry, B. Leonard for sharing unpublished data, M. Shales for help with figures, and B. Chesebro, D. Gabuzda, J. Lingappa, M. Malim, K. Wehrly, X. F. Yu, A. Bullock, B. Schulman and the AIDS Research and Reference Reagent Program for reagents. This research was funded by grants from QB3 at University of California, San Francisco, and the National Institutes of Health (P50 GM082250, P01 AI090935 and P50 GM081879 to N.J.K.; U54 RR022220 to A.S.; R01 AI064046 and P01 GM091743 to R.S.H.; P50 GM082250 to J.D.G. and C.S.C.; P41RR001614 and P50GM081879 to A.B.). N.J.K. is a Searle Scholar and a Keck Young Investigator.

Author Contributions K.S., R.S.L. and E.K. made equal secondary contributions to this work. S.J. and K.F.S. generated the Vif protein–protein interaction map (Fig. 1); S.J. performed the co-immunoprecipitation confirmation assays (Supplementary Fig. 1); P.C. developed and implemented the MiST scoring system (Fig. 1c); S.J. and E.K. performed double purification analyses (Fig. 1c, d); C.M. and J.K. performed immunoprecipitation analyses (Fig. 1f, g); D.Y.K., L.Y. and D.S. reconstituted the Vif E3 ligase from recombinant components and performed ubiquitination assays (Fig. 2 and Supplementary Figs 2–4); M.L. expressed and purified A3 proteins and did *in vitro* pulldowns (Fig. 2); K.S., J.F.H. and R.S.L. performed CBF-β knockdown, complementation and virus infectivity experiments (Fig. 3 and Supplementary Figs 5–7); and B.D.A. and J.F.H. did the CBF-β–Vif co-immunoprecipitation experiments (Supplementary Fig. 8). A.B., A.S., C.S.C., R.S.H., J.D.G. and N.J.K. supervised the research; S.J., D.Y.K., J.F.H., K.S., R.S.H., J.D.G. and N.J.K. wrote and revised the manuscript.

Author Information Reprints and permissions information is available at www.nature.com/reprints. The authors declare no competing financial interests. Readers are welcome to comment on the online version of this article at www.nature.com/nature. Correspondence and requests for materials should be addressed to R.S.H. (rsh@umn.edu), J.D.G. (jdgross@cgl.ucsf.edu) or N.J.K. (krogan@cmp.ucsf.edu).